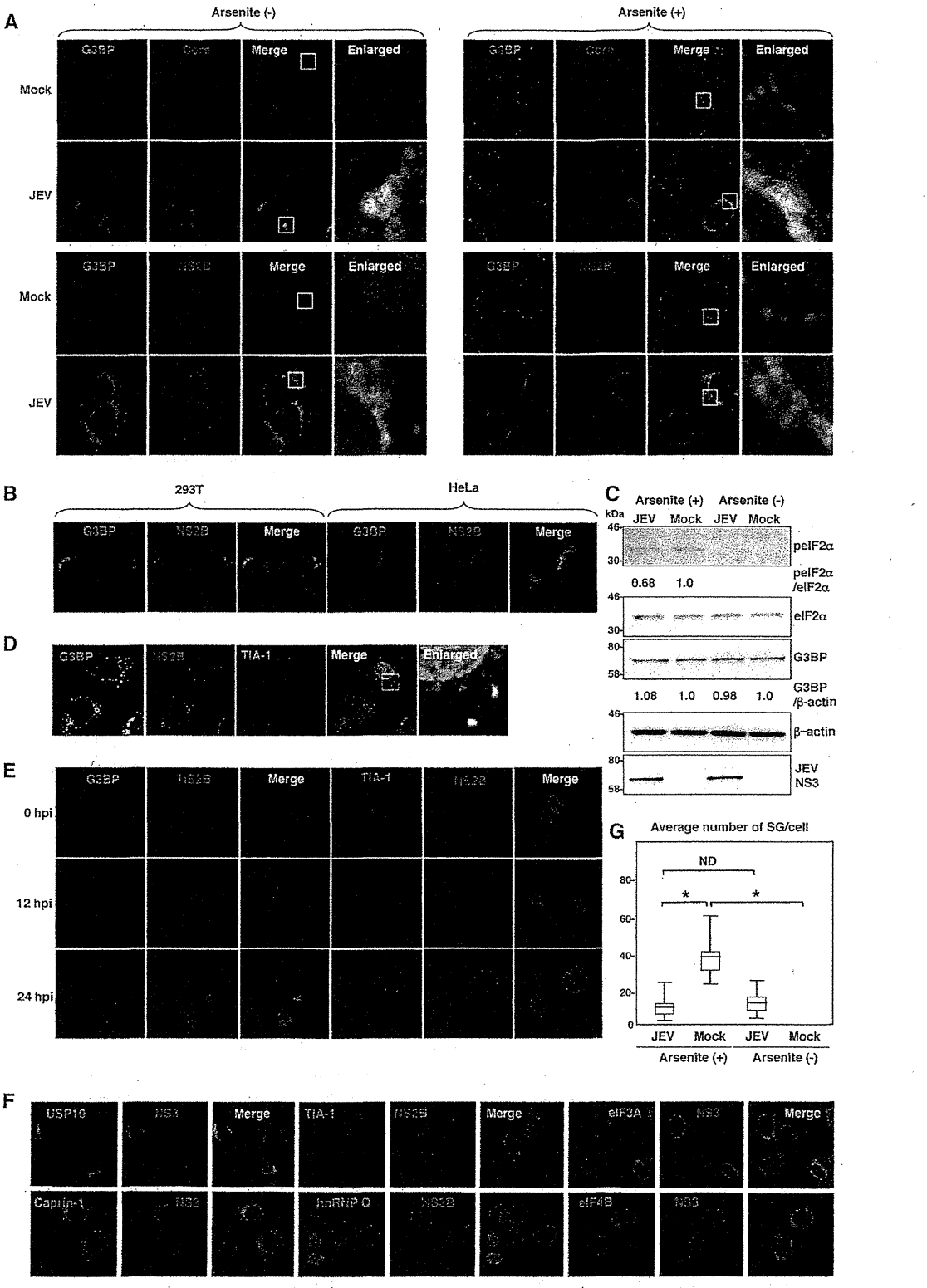

FIG 1 Dynamics of SG-associated factors during JEV infection. (A) Huh7 cells infected with JEV at an MOI of 0.5 were treated with or without 1.0 mM sodium arsenite for 30 min at 37°C, and the levels of expression of G3BP and JEV core protein/NS2B were determined at 24 h postinfection by immunofluorescence analysis with mouse anti-G3BP MAb and rabbit anti-core protein or anti-NS2B PAb, followed by AF488-conjugated anti-mouse IgG (Invitrogen) and AF594-conjugated anti-rabbit IgG, respectively. Cell nuclei were stained with DAPI (blue). (B) Cellular localizations of G3BP and JEV NS2B in 293T and HeLa cells infected with JEV were determined at 24 h postinfection by immunofluorescence analysis with mouse anti-G3BP MAb and rabbit anti-NS2B PAb, followed by AF488-conjugated anti-mouse IgG and AF594-conjugated anti-rabbit IgG, respectively. Cell nuclei were stained with DAPI (blue). (C) Phosphorylation of eIF2α in cells prepared as described in panel A was determined by immunoblotting using the indicated antibodies. The band intensities were quantified by ImageJ

a single-stranded positive-sense RNA genome of approximately 11 kb. The genomic RNA carries a single large open reading frame, and a polyprotein translated from the genome is cleaved co- and posttranslationally by host and viral proteases to yield three structural proteins, the core, precursor membrane (PrM), and envelop (E) proteins, and seven nonstructural (NS) proteins, NS1, NS2A, NS2B, NS3, NS4A, NS4B, and NS5 (13). PrM is further cleaved by the multibasic protease, furin, and matured to membrane (M) protein. The core, M, and E proteins are components of extracellular mature virus particles. NS proteins are not incorporated into particles and are thought to be involved in viral replication, which occurs in close association with ER-derived membranes (14). Previous reports have shown that WNV and DENV inhibit SG formation by sequestering TIA-1 and TIAR through specific interaction with viral RNA (15, 16). In addition, the membrane structure induced by WNV infection was suggested to prevent PKR activation and avoid induction of SG formation (17). In this study, we show that JEV core protein plays an important role in inhibition of SG formation. JEV core protein recruited several SG-associated proteins, including G3BP and USP10, through an interaction with Caprin-1 and suppressed SG formation. Furthermore, a mutant JEV carrying a core protein incapable of binding to Caprin-1 exhibited lower propagation *in vitro* and lower pathogenicity in mice than the wild-type (WT) JEV, suggesting that inhibition of SG formation by the core protein is crucial to antagonize host defense. These results reveal a novel strategy of JEV to inhibit SG formation through an interaction with Caprin-1 and facilitate viral propagation.

MATERIALS AND METHODS

Plasmids. Plasmids encoding FLAG-tagged JEV core protein (pCAGPM-FLAG-Core) and hemagglutinin (HA)-tagged JEV proteins (pCAGPM-HA-JEV proteins) were generated as previously described (18, 19). The cDNA of the core protein of JEV AT31 (amino acid residues 2 to 105) was amplified from the pCAGPM-FLAG-Core plasmid by PCR and cloned into pET21b (Novagen-Merck, Darmstadt, Germany) for expression in bacteria as a His-tagged protein and in pCAG-MCS2-FOS for expression in mammalian cells as a FLAG-One-STrEP (FOS)-tagged protein. The resulting plasmids were designated pET21b-Core-His and pCAG-Core-FOS, respectively. The cDNA of the core protein of DENV2 (amino acid residues 2 to 100) was amplified from the pCAG/FLAG-DEN2C-HA plasmid (19) by PCR and cloned into pCAGPM-N-FLAG. The cDNA of human Caprin-1 was amplified from 293T cells by reverse transcription-PCR (RT-PCR) and cloned into pCAGPM-N-HA (20) and pGEX 6P-1 (GE Healthcare, Buckinghamshire, United Kingdom) for expression in bacteria as a glutathione *S*-transferase (GST) fusion protein and designated pCAGPM-HA-Caprin-1 and pGEX-GST-Caprin-1, respectively. The cDNAs of human G3BP1 and USP10 were also amplified from 293T cells by RT-PCR and cloned into pCAGPM-N-HA. The nucleotide residues of the adenine at 384, adenine at 385, cytosine at 387, and guanine at 388 of the JEV genome in pMWATG1 were replaced with guanine, cytosine, guanine, and cytosine, respectively, by PCR-based mutagenesis to change Lys^{97} and Arg^{98} of the core protein to Ala, yielding pMWAT/KR9798A. The cDNA of the mutant core protein was also cloned into pCAGPM-N-FLAG and pET21b. To generate stable cell lines expressing *Aequorea coerulescens* green fluorescent protein (AcGFP)-fused Caprin-1, the cDNA of human Caprin-1 was amplified by RT-PCR and cloned into pAcGFP N1 (Clontech, Mountain View, CA), and the Caprin-1-AcGFP gene was subcloned into the lentiviral vector pCSII-EF-RfA (21) and designated pCSII-EF-Caprin-1-AcGFP. All plasmids were confirmed by sequencing with an ABI Prism 3130 genetic analyzer (Applied Biosystems, Tokyo, Japan).

Cells and stress treatment. Mammalian cell lines, Vero (African green monkey kidney), 293T (human kidney), Huh7 (human hepatocellular carcinoma), and HeLa (human cervical carcinoma), were maintained in Dulbecco's modified Eagle's minimal essential medium (DMEM) (Sigma, St. Louis, MO) supplemented with 100 U/ml penicillin, 100 mg/ml streptomycin, nonessential amino acids (Sigma), and 10% fetal bovine serum (FBS). The mosquito cell line C6/36 (*Aedes albopictus*) was grown in Leibovitz's L-15 medium with 10% FBS. Huh7 cells were transduced with a lentiviral vector expressing Caprin-1-AcGFP and AcGFP and designated Huh7/Caprin-1-AcGFP and Huh7/AcGFP, respectively. For induction of SGs, cells were treated with sodium arsenite at a final concentration of 1.0 mM in the culture medium for 30 min prior to fixation or lysis of the cells. SG formation was defined morphologically by immunostaining using anti-SG-related factor antibodies described below. Cell viability was determined by using CellTiter-Glo (Promega, Madison, WI) according to the manufacturer's instruction.

Viruses. The wild-type and 9798A mutant of the JEV AT31 strain were generated by the transfection of pMWATG1 and pMWAT/KR9798A, respectively, as described previously (22). Viral infectivity was determined by an immunostaining focus assay as described previously (20), and the results are expressed in focus-forming units (FFU). JEV and DENV serotype 2 New Guinea C strain were amplified in C6/36 cells.

Antibodies. Anti-JEV core rabbit polyclonal antibody (PAb) and anti-JEV NS3 mouse monoclonal antibody (MAb) were prepared as described previously (20, 23). Anti-JEV NS2B rabbit PAb was generated with synthetic peptides of JEV NS2B at Scrum, Inc. (Tokyo, Japan). Anti-DENV core protein rabbit PAb was prepared by using a GST-fused recombinant protein containing amino acid residues 2 to 100 of the DENV core protein. Anti-FLAG mouse MAb (M2) and rabbit PAb and anti-β-actin mouse MAb were purchased from Sigma. Anti-hnRNP Q mouse MAb (ab10687), anti-USP10 rabbit PAb (ab70895), and anti-eIF4B rabbit PAb (ab78916) were purchased from Abcam (Cambridge, United Kingdom). Anti-eIF2α, anti-phospho-eIF2α, and anti-eIF3A rabbit PAbs were purchased from Cell Signaling Technology (Danvers, MA). Anti-HA mouse MAb (HA11), anti-HA rat MAb (3F10), anti-His mouse MAb, anti-GFP mouse MAb (JL-8), anti-JEV envelope protein mouse MAb (6B4A-10), anti-G3BP mouse MAb, anti-TIA-1 goat PAb, anti-Caprin-1 rabbit PAb, and anti-dsRNA mouse MAb were purchased from Covance (Richmond, CA), Roche (Mannheim, Germany), R&D Systems (Minneapolis, MN), Clontech, Chemicon (Temecula, CA), BD Biosciences (Franklin Lakes, NJ), Santa Cruz (Santa Cruz, CA), Proteintech (Chicago, IL), and Bio-

software (NIH, Bethesda, MD), and the relative levels for the indicated proteins are shown based on the level of the mock-infected cells. (D) Cellular localizations of G3BP, NS2B, and TIA-1 in Huh7 cells infected with JEV were determined at 24 h postinfection by immunofluorescence analysis with mouse anti-G3BP MAb, rabbit anti-NS2B PAb, and goat anti-TIA-1 PAb, followed by AF488-conjugated anti-mouse IgG, AF594-conjugated anti-rabbit IgG, and AF633-conjugated anti-goat IgG, respectively. Cell nuclei were stained with DAPI (gray). (E) Dynamics of G3BP and TIA-1 during JEV infection. Huh7 cells infected with JEV were immunostained at 0, 12, and 24 h postinfection (hpi) with mouse anti-G3BP MAb or goat anti-TIA-1 PAb and rabbit anti-NS2B PAb, followed by AF488-conjugated anti-mouse IgG or AF488-conjugated anti-goat IgG and AF594-conjugated anti-rabbit IgG, respectively. Cell nuclei were stained with DAPI (blue). (F) Cellular localization of SG-associated proteins (USP10, Caprin-1, TIA-1, hnRNP Q, eIF3A, and eIF4B) (green, AF488-conjugated secondary antibody) and JEV NS2B/NS3 (red, AF-594-conjugate secondary antibody) in Huh7 cells infected with JEV was determined by immunoblotting at 24 h postinfection. Cell nuclei were stained with DAPI (blue). (G) Numbers of G3BP-positive foci in 30 cells prepared as described in panel A were counted for each experimental condition. Lines, boxes, and error bars indicate the means, 25th to 75th percentiles, and 95th percentiles, respectively. The significance of differences between the means was determined by a Student's *t* test.*, $P < 0.01$; ND, no significant difference.

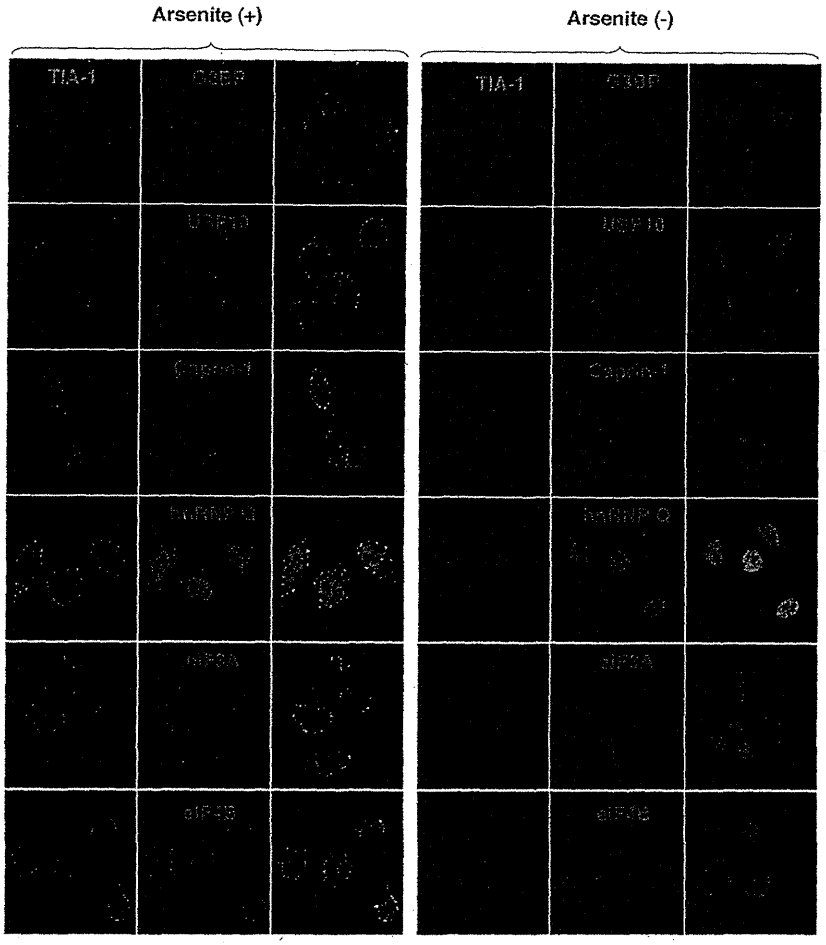

FIG 2 Each SG-associated factor forms SGs under oxidative stress. After treatment with 1.0 mM sodium arsenite for 30 min at 37°C, Huh7 cells were subjected to immunofluorescence analysis with the indicated primary antibodies, followed by AF488-conjugated anti-goat IgG and AF594-conjugated anti-mouse or rabbit IgG. Cell nuclei were stained with DAPI (blue).

center (Szirak, Hungary), respectively. Alexa Fluor (AF)-conjugated secondary antibodies were purchased from Invitrogen (Carlsbad, CA).

Immunofluorescence microscopy. Huh7 cells were fixed in 4% paraformaldehyde in phosphate-buffered saline (PBS) for 15 min at room temperature. After cells were quenched for 10 min with PBS containing 50 mM ammonium chloride (NH_4Cl), they were permeabilized with 0.2% Triton X-100 in PBS for 10 min and blocked with PBS containing 2% bovine serum albumin (BSA) for 30 min at room temperature. The cells were then incubated with the antibodies indicated in the figure legends. Nuclei were stained with 4′,6′-diamidino-2-phenylindole (DAPI). The samples were examined by a Fluoview FV1000 laser scanning confocal microscope (Olympus, Tokyo, Japan).

Transfection, immunoprecipitation, and immunoblotting. Plasmids were transfected into 293T or Huh7 cells by use of TransIT LT1 (Mirus, Madison, WI), and cells collected at 24 h posttransfection were subjected to immunostaining, immunoprecipitation, and/or immunoblotting as described previously (24). The immunoprecipitates were boiled in sodium dodecyl sulfate (SDS) sample buffer and subjected to SDS-polyacrylamide gel electrophoresis (SDS-PAGE). The proteins were transferred to polyvinylidene difluoride membranes (Millipore, Bedford, MA) and incubated with the appropriate antibodies. The immune complexes were visualized with SuperSignal West Femto substrate (Thermo Scientific, Rockford, IL) and detected by use of an LAS-3000 image analyzer system (Fujifilm, Tokyo, Japan).

FOS-tagged purification and mass spectrometry. pCAG-Core-FOS or empty vector was transfected into 293T cells, harvested at 24 h posttransfection, washed with cold PBS, suspended in cell lysis buffer (20 mM Tris-HCl, pH 7.4, 135 mM NaCl, 1% Triton X-100, and protease inhibitor cocktail [Complete; Roche]), and centrifuged at 14,000 × *g* for 20 min at 4°C. The supernatant was pulled down using 50 μl of STrEP-Tactin Sepharose (IBA, Gottingen, Germany) equilibrated with cell lysis buffer for 2 h at 4°C. The affinity beads were washed three times with cell lysis buffer and suspended in 2× SDS-PAGE sample buffer. The proteins were subjected to SDS-PAGE, followed by Coomassie brilliant blue (CBB) staining using CBB Stain One (Nakalai Tesque, Kyoto, Japan). The gels were divided into 10 pieces, and each fraction was trypsinized and subjected to liquid chromatography-tandem mass spectrometry (LC-MS/MS) analysis to identify coimmunoprecipitated proteins. All of the proteins in gels were identified comprehensively, and the proteins detected in cells transfected with pCAG-Core-FOS but not in those with empty vector were regarded as candidates for binding partners of JEV core.

Gene silencing. A commercially available small interfering RNA (siRNA) pool targeting Caprin-1 (siGENOME SMARTpool, human Caprin1) and control nontargeting siRNA were purchased from Dharmacon (Buckinghamshire, United Kingdom) and transfected into 293T cells using Lipofectamine RNAiMAX (Invitrogen) according to the manufacturer's protocol.

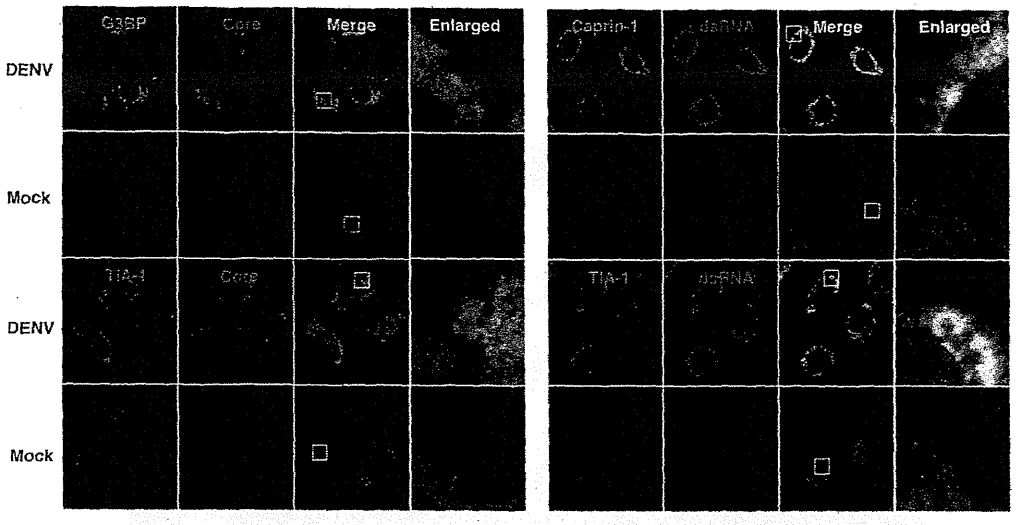

FIG 3 Subcellular localizations of the SG-associated proteins during DENV infection. Cellular localizations of G3BP, Caprin-1, and TIA-1 (green, AF488-conjugated secondary antibody) and viral components (core protein and dsRNA) (red, AF-594-conjugate secondary antibody) in Huh7 cells infected with DENV were determined by immunofluorescence analysis using the appropriate antibodies at 48 h postinfection. Cell nuclei were stained with DAPI (blue).

Preparation of recombinant proteins and GST pulldown assay. His-tagged JEV core protein (core-His) was purified as described in a previous report (25). Briefly, core-His was expressed in *Escherichia coli* (*E. coli*) Rosetta-gami 2(DE3) strain cells (Novagen-Merck) transformed with pET21b-Core-His (WT or 9798A). Bacteria grown to an optical density at 600 nm of 0.6 were induced with 0.5 mM isopropyl-β-D-thiogalactopyranoside (IPTG), incubated for 5 h at 37°C with shaking, collected by centrifugation at 6,000 × *g* for 10 min, lysed in 10 ml of bacteria lysis buffer (50 mM Tris-HCl, pH 7.4, 150 mM NaCl, 1 mM EDTA, 1% Triton X-100, and protease inhibitor cocktail [Complete; Roche]) by sonication on ice, and centrifuged at 10,000 × *g* for 15 min. The supernatant containing core-His was subjected to ammonium sulfate fractionation, followed by cation exchange chromatography with a HiTrap SP column (GE Healthcare). The eluted core-His recombinant protein was dialyzed with 50 mM Tris-HCl buffer containing 150 mM NaCl at 4°C overnight. GST-fused Caprin-1 (GST-Caprin-1) was expressed in *E. coli* BL21(DE3) cells transformed with pGEX-GST-Caprin-1. Bacteria grown to an optical density at 600 nm of 1.0 were induced with 0.1 mM IPTG, incubated for 5 h at 25°C with shaking, collected by centrifugation at 6,000 × *g* for 10 min, lysed in 10 ml of bacteria lysis buffer by sonication on ice, and centrifuged at 10,000 × *g* for 15 min. The supernatant was mixed with 200 μl of glutathione-Sepharose 4B beads (GE Healthcare) equilibrated with bacteria lysis buffer for 1 h at room temperature, and then the beads were washed five times with lysis buffer. Twenty micrograms of GST-Caprin-1 or GST was mixed with equal volumes of the purified core-His for 2 h at 4°C with gentle agitation. The beads were washed five times with bacteria lysis buffer and then suspended in SDS-PAGE sample buffer.

Mouse experiments. Experimental infections were approved by the Committee for Animal Experiment of RIMD, Osaka University (H19-2-0). Female ICR mice (3 weeks old) were purchased from CLEA Japan (Tokyo, Japan) and kept in specific pathogen-free environments. Groups of mice ($n = 10$) were intraperitoneally inoculated with 5×10^4 FFU (100 μl) of the viruses. The mice were observed for 3 weeks after inoculation to determine survival rates. To examine viral growth in the brain, 5×10^4 FFU of the viruses were intraperitoneally administered to the groups of mice ($n = 3$). At 7 days postinfection, mice were euthanized, and the cerebrums were collected. The infectious titers in the homogenates of the cerebrums were determined in Vero cells as described above.

RESULTS

JEV infection confers resistance to SG induction. To examine the formation of SGs in cells infected with JEV, Huh7 cells were infected with JEV at a multiplicity of infection (MOI) of 0.5, and the expression of JEV proteins and an accepted marker for SGs, G3BP, was determined by immunofluorescence analysis at 24 h postinfection. G3BP was mainly accumulated in the perinuclear region and partially colocalized with the JEV core protein, while only partial colocalization with the NS2B protein was also observed (Fig. 1A, left). In addition, a few small G3BP-positive foci were scattered in the cytoplasm. This accumulation of G3BP was observed in not only Huh7 cells but also other cell lines, i.e., 293T and HeLa cells, infected with JEV (Fig. 1B). However, the expression level of G3BP in cells infected with JEV was comparable to that in mock-infected cells (Fig. 1C). To further investigate SG induction by JEV infection, expression of TIA-1, another SG marker, was examined. Although accumulation of TIA-1 in the perinuclear region was not observed, a few TIA-1-positive foci were observed in the JEV-infected cells and were colocalized with G3BP and JEV NS2B, indicating that SG foci were induced in cells infected with JEV (Fig. 1D). The accumulation of G3BP and the aggregation of TIA-1, indicating SG formation, appeared at 24 h postinfection in accord with the expression of viral proteins (Fig. 1E). We further examined the dynamics of other SG-associated factors in cells infected with JEV. Each factor formed clear SGs in cells treated with sodium arsenite, a potent SG inducer eliciting oxidative stress (Fig. 2). As shown in Fig. 1F, three distinct patterns of the subcellular localization of SG components were observed. USP10 and Caprin-1 were accumulated in the perinuclear region and also formed a few small foci scattered throughout the cytoplasm, as seen for G3BP; TIA-1 and hnRNP Q formed cytoplasmic foci but were not accumulated in the perinuclear region; and subcellular localization of eIF3A and eIF4B was not changed. The cytoplasmic foci were confirmed as SGs by immunofluorescence analyses using specific antibodies to SG-associated factors (data not shown). Taken together, these results indicate that JEV infection induces accumulation of several RBPs and formation of a few SGs.

It has been shown previously that infection with WNV or DENV confers resistance to SG formation induced by sodium arsenite (15). To determine the effect of JEV infection on the SG

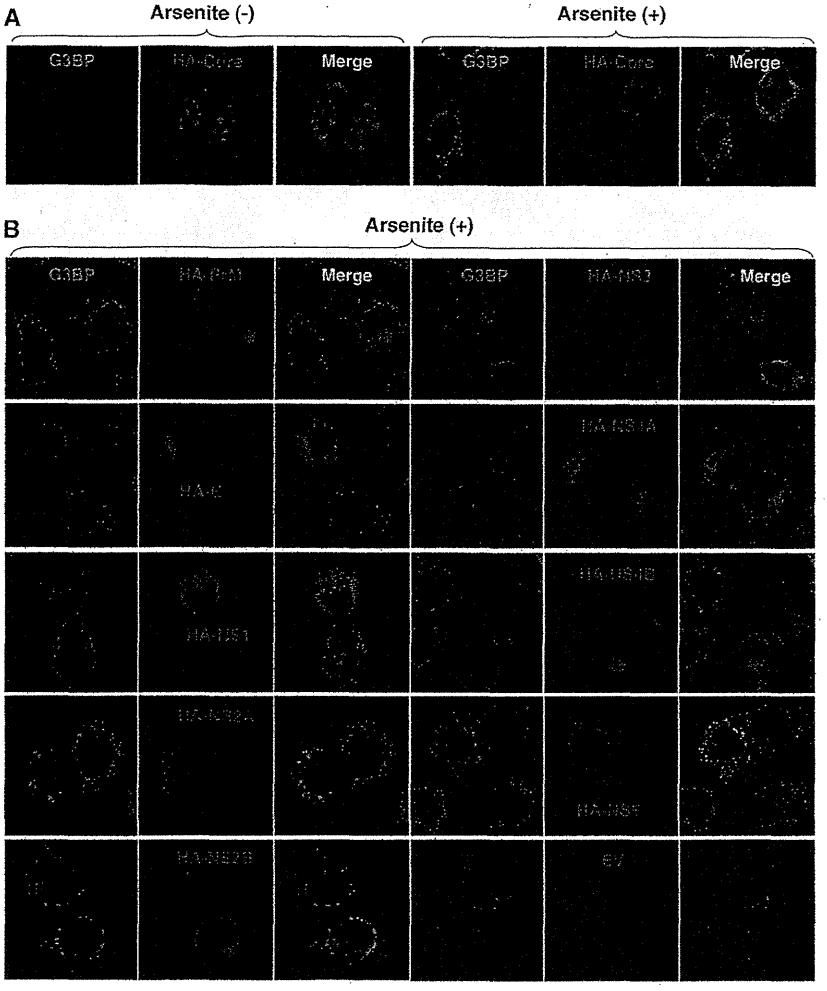

FIG 4 Inhibition of the arsenite-induced SG formation by the expression of JEV proteins. (A) Huh7 cells transfected with a plasmid, pCAGPM-HA-Core, were treated with or without 1.0 mM sodium arsenite for 30 min at 37°C, and the cellular localizations of G3BP and HA-Core were determined at 24 h posttransfection by immunofluorescence analysis with mouse anti-G3BP MAb and rat anti-HA MAb, followed by AF488-conjugated anti-mouse IgG and AF594-conjugated anti-rat IgG, respectively. Cell nuclei were stained with DAPI (blue). (B) Huh7 cells, which were separately transfected with a plasmid expressing an individual viral protein (pCAGPM-HA-JEV protein) as indicated in the figure, were treated with 1.0 mM sodium arsenite for 30 min at 37°C and subjected to an immunofluorescence assay using mouse anti-G3BP MAb and rat anti-HA MAb, followed by AF488-conjugated anti-mouse IgG and AF594-conjugated anti-rat IgG, respectively. Cell nuclei were stained with DAPI (blue).

formation induced by sodium arsenite, JEV-infected cells were treated with 0.5 mM sodium arsenite for 30 min at 24 h postinfection. Although many G3BP-positive foci were observed in mock-infected cells by the treatment with sodium arsenite, accumulation of G3BP in the perinuclear region was observed in the JEV-infected cells (Fig. 1A, right), and the numbers of G3BP-positive foci in the JEV-infected cells were less than those in the mock-infected cells (Fig. 1G). Although it has been reported that a significant reduction of the phosphorylation at Ser^{51} of eIF2α in cells treated with arsenite was induced by infection with WNV (15), the phosphorylation of eIF2α was slightly suppressed in the JEV-infected cells (Fig. 1C). Furthermore, while previous studies reported that Caprin-1 and TIA-1 were colocalized with dsRNA in cells infected with DENV (15, 26), no colocalization of G3BP or TIA-1 with the DENV core protein was observed in the present study (Fig. 3), suggesting that the mechanisms of the viral circumvention of SG formation in cells infected with JEV are different from those in cells infected with WNV and DENV.

JEV core protein suppresses SG formation induced by sodium arsenite. To elucidate the molecular mechanisms of suppression of SG formation induced by sodium arsenite during JEV infection, we tried to identify which viral protein(s) is responsible for the SG inhibition. Since G3BP was colocalized with JEV core protein, we first examined the involvement of the core protein in the perinuclear accumulation of G3BP and in the suppression of SG formation. The expression of JEV core protein alone induced the accumulation of G3BP in the perinuclear region (Fig. 4A, left panel) and suppressed sodium arsenite-induced SG formation (Fig. 4A, upper right cell in the right panel), similarly to JEV infection. In contrast, inhibition of SG formation induced by sodium arsenite was not observed in cells expressing other JEV proteins (Fig. 4B). These results suggest that JEV core protein is responsible for the circumvention of the SG formation observed in cells infected with JEV.

JEV core protein directly interacts with Caprin-1, an SG-associated cellular factor. Since JEV core protein was suggested to

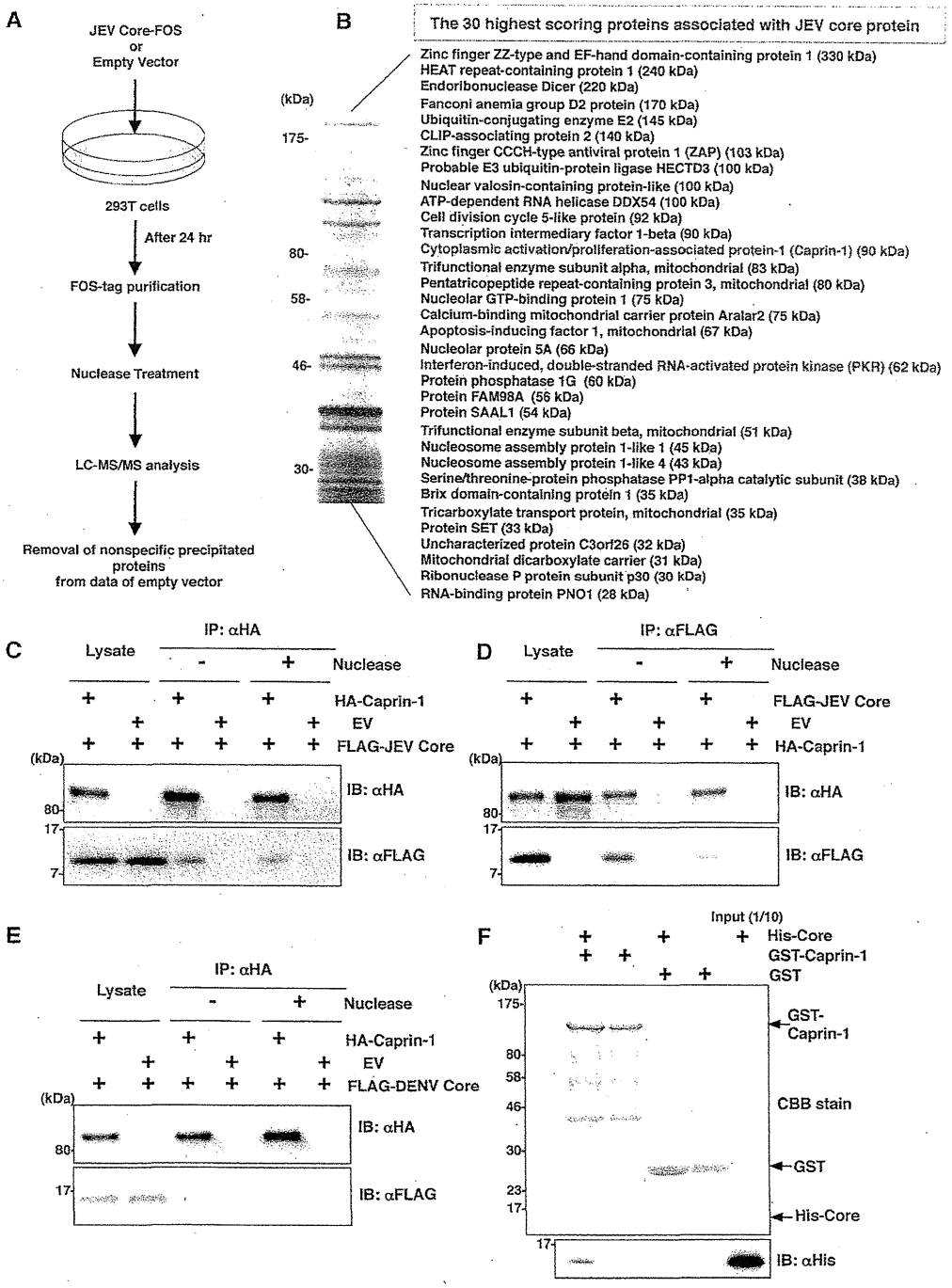

FIG 5 JEV core protein directly interacts with Caprin-1, an SG-associated cellular factor. (A) Identification of host cellular proteins associated with JEV core protein by FOS-tagged purification and LC-MS/MS analysis. Overview of the FOS-tagged purification of cellular proteins associated with JEV core protein. (B) The 30 candidate proteins as binding partners of JEV core protein exhibiting high scores are listed. PKR and Caprin-1 are indicated in red. (C and D) FLAG-JEV core protein and HA-Caprin-1 were coexpressed in 293T cells, and the cell lysates harvested at 24 h posttransfection were treated with or without micrococcal nuclease for 30 min at 37°C and immunoprecipitated (IP) with anti-HA (αHA) or anti-FLAG (αFLAG) antibody, as indicated. The precipitates were subjected to immunoblotting (IB) to detect coprecipitated counterparts. (E) FLAG-DENV core protein was coexpressed with HA-Caprin-1 in 293T cells, immunoprecipitated with anti-HA antibody, and immunoblotted with anti-HA or anti-FLAG antibody. (F) His-tagged JEV core protein was incubated with either GST-fused Caprin-1 or GST for 2 h at 4°C, and the precipitates obtained by GST pulldown assay were subjected to CBB staining and immunoblotting with anti-His antibody.

participate in the inhibition of SG formation, we tried to identify cellular factors associated with the core protein by LC-MS/MS analysis, as shown in Fig. 5A. Among the 30 factors with the best scores, two SG-associated proteins, PKR (Mascot search score, 206) and Caprin-1 (Mascot search score, 153), were identified as binding partners of JEV core protein (Fig. 5B). Although PABP1, hnRNP Q, Staufen, G3BP, and eIF4G were also identified, their scores were lower than those of PKR and Caprin-1. Because the

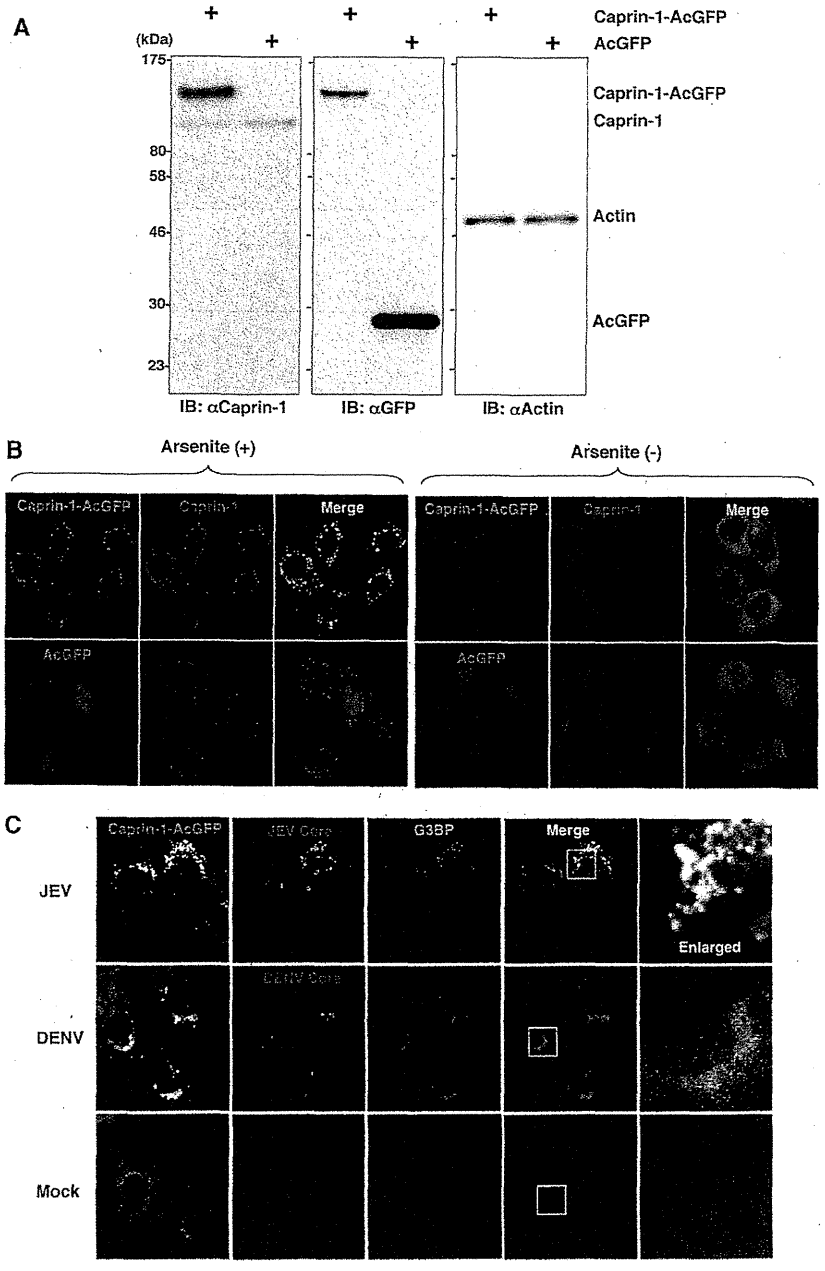

FIG 6 Caprin-1 is colocalized with the JEV core protein in the perinuclear region. (A) Expression of Caprin-1 fused with AcGFP (Caprin-1-AcGFP), Caprin-1, actin, or AcGFP in lentivirally transduced Huh7 cells was determined by immunoblotting using the appropriate antibodies. (B) Subcellular localization of Caprin-1-AcGFP or AcGFP (green) and endogenous Caprin-1 (red) in cells treated with/without 1.0 mM sodium arsenite for 30 min at 37°C was determined by immunofluorescence assay with rabbit anti-Caprin-1 PAb and AF594-conjugated anti-rabbit IgG. Cell nuclei were stained with DAPI (blue). (C) Huh7/Caprin-1-AcGFP cells were infected with either JEV or DENV at an MOI of 0.5, and the cellular localizations of JEV and DENV core (red) with Caprin-1-AcGFP and G3BP (blue) were determined at 24 h and 48 h postinfection, respectively. Cells were stained with mouse anti-G3BP MAb and rabbit anti-JEV or DENV core protein PAb, followed by AF633-conjugated anti-mouse IgG and AF594-conjugated anti-rabbit IgG, respectively, and examined by immunofluorescence analysis.

results shown in Fig. 1B suggest that the inhibition of SG formation takes place downstream of eIF2α phosphorylation, we focused on Caprin-1 as a key factor involved in the inhibition of SG formation in cells infected with JEV. To confirm the specific interaction of JEV core protein with Caprin-1, FLAG-JEV core protein and HA-Caprin-1 were coexpressed and immunoprecipitated with anti-HA or anti-FLAG antibody in the presence or absence of nuclease. FLAG-JEV core protein was coprecipitated with HA-Caprin-1 irrespective of nuclease treatment (Fig. 5C and D), suggesting that the interaction between JEV core protein and Caprin-1 is a protein-protein interaction. On the other hand, FLAG-DENV core protein was not coprecipitated with HA-Caprin-1 (Fig. 5E), indicating that the interaction with Caprin-1 was specific for JEV core protein. Next, the direct interaction be-

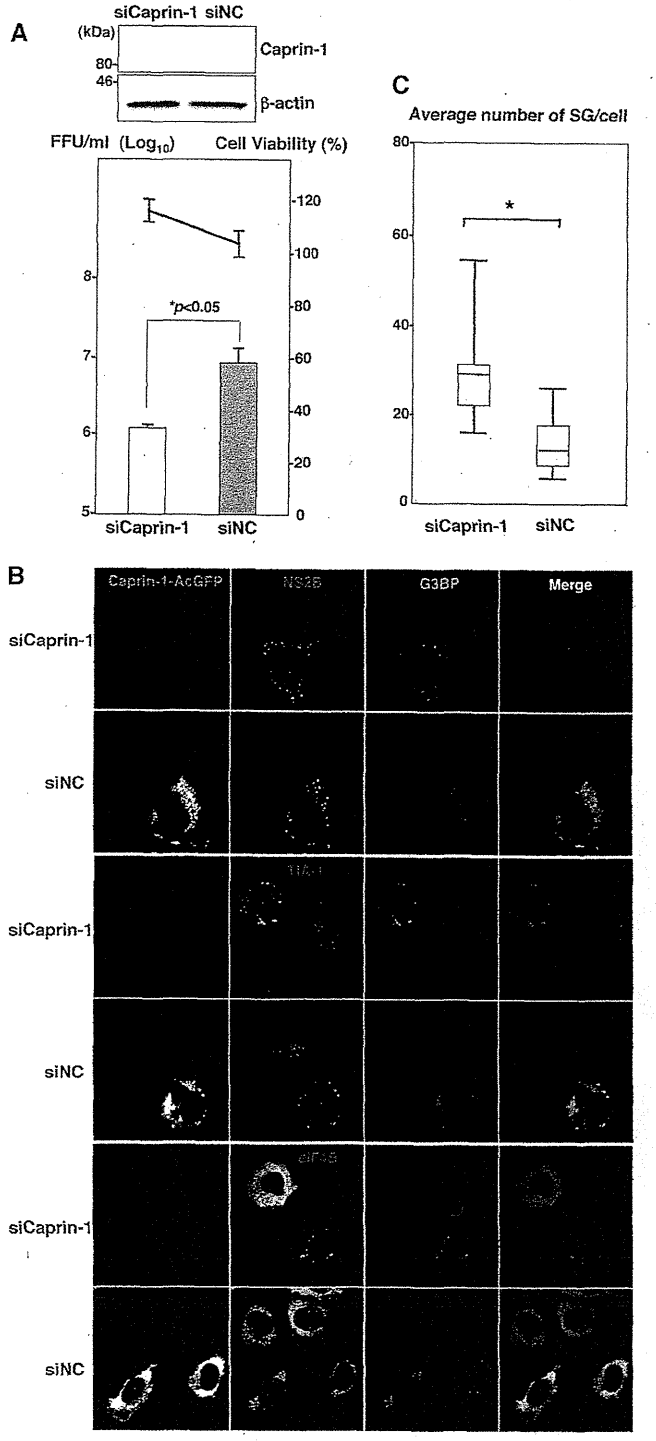

FIG 7 Knockdown of Caprin-1 cancels SG inhibition during JEV infection and suppresses viral propagation. (A) (Upper) The levels of expression of Caprin-1 in cells transfected with either siCaprin-1 or siNC was determined by immunoblotting using anti-Caprin-1 and anti-β-actin antibodies at 72 h posttransfection (top panel). At 48 h posttransfection with either siCaprin-1 or siNC, Huh7/Caprin-1-AcGFP cells were inoculated with JEV at an MOI of 0.5. At 24 h postinfection (72 h posttransfection), the infectious titers in the supernatants were determined by focus-forming assay in Vero cells (bottom panel, bar graph). Cell viability was determined at 72 h posttransfection and calculated as a percentage of the viability of cells treated with siNC (bottom panel, line graph). The results shown are from three independent assays, with the error bars representing the standard deviations. (B) At 48 h posttransfection with either siCaprin-1 or siNC, Huh7/Caprin-1-AcGFP cells were inoculated with JEV at an MOI of 0.5. The cellular localizations of SG-associated factors and JEV NS2B were determined at 24 h postinfection (72 h posttransfection) by immunofluorescence analysis with mouse anti-G3BP MAb and rabbit anti-NS2B PAb, rabbit anti-eIF4B PAb, or goat anti-TIA-1 PAb, followed by AF633-conjugated anti-mouse IgG and AF594-conjugated anti-rabbit IgG or AF594-conjugated anti-goat IgG, respectively. (C) Numbers of G3BP-positive foci in 30 cells prepared as described in panel B were counted. Lines, boxes, and error bars indicate the means, 25th to 75th percentiles, and 95th percentiles, respectively. The significance of differences between the means was determined by a Student's *t* test. *, $P < 0.01$.

tween JEV core protein and Caprin-1 was examined by a GST-pulldown assay using purified proteins expressed in bacteria. The His-tagged core protein was coprecipitated with GST-tagged Caprin-1, suggesting that JEV core protein directly interacts with Caprin-1 (Fig. 5F).

To further determine the cellular localization of Caprin-1 in JEV-infected cells, Caprin-1 fused with AcGFP (Caprin-1-AcGFP) was lentivirally expressed in Huh7 cells. The levels of expression and recruitment of Caprin-1-AcGFP into SGs were determined by immunoblotting and immunofluorescence analysis, respectively (Fig. 6A and B). In cells infected with JEV, Caprin-1-AcGFP was concentrated in the perinuclear region and colocalized with core protein and G3BP, while no colocalization of the proteins was observed in cells infected with DENV (Fig. 6C), suggesting that Caprin-1 directly interacts with JEV core protein in the perinuclear region of the infected cells.

Knockdown of Caprin-1 cancels SG inhibition during JEV infection and suppresses viral propagation. To assess the biological significance of the interaction of JEV core protein with Caprin-1 in JEV propagation, the expression of Caprin-1 was suppressed by using Caprin-1-specific siRNAs (siCaprin-1). Transfection of siCaprin-1 efficiently and specifically knocked down the expression of Caprin-1 with a slight increase of cell viability and decreased the production of infectious particles in the culture supernatants of cells infected with JEV, in comparison with those treated with a control siRNA (siNC) (Fig. 7A). Furthermore, immunofluorescence analyses revealed that knockdown of Caprin-1 increased the number of G3BP-positive granules colocalized with SG-associated factors, including TIA-1 and eIF4B, and inhibited the G3BP concentration in the perinuclear region (Fig. 7B and C). These results suggest that knockdown of Caprin-1 suppresses JEV propagation through the induction of SG formation.

Lys^{97} and Arg^{98} in the JEV core protein are crucial residues for the interaction with Caprin-1. To determine amino acid residues of the core protein that are required for the interaction with Caprin-1, we constructed a putative model based on the structural information of the DENV core protein previously resolved by nuclear magnetic resonance (NMR) (27), as shown in Fig. 8A. Based on this model, we selected hydrophobic amino acids, which were located on the solvent-exposed side in the α1 and α4 helices, as amino acid residues responsible for the binding to host proteins. Amino acid substitutions in each of the α-helices shown in Fig. 8B were designed in the context of FLAG-Core (Mα1 and Mα4), and the interaction of FLAG-Core mutants with Caprin-1 was examined by immunoprecipitation analysis. WT and Mα1, but not Mα4, core proteins were immunoprecipitated with Caprin-1 (Fig. 8B). To determine the amino acids responsible for interaction with Caprin-1, further alanine substitutions were introduced in the α4 helix, and the interaction was examined by immunopre-

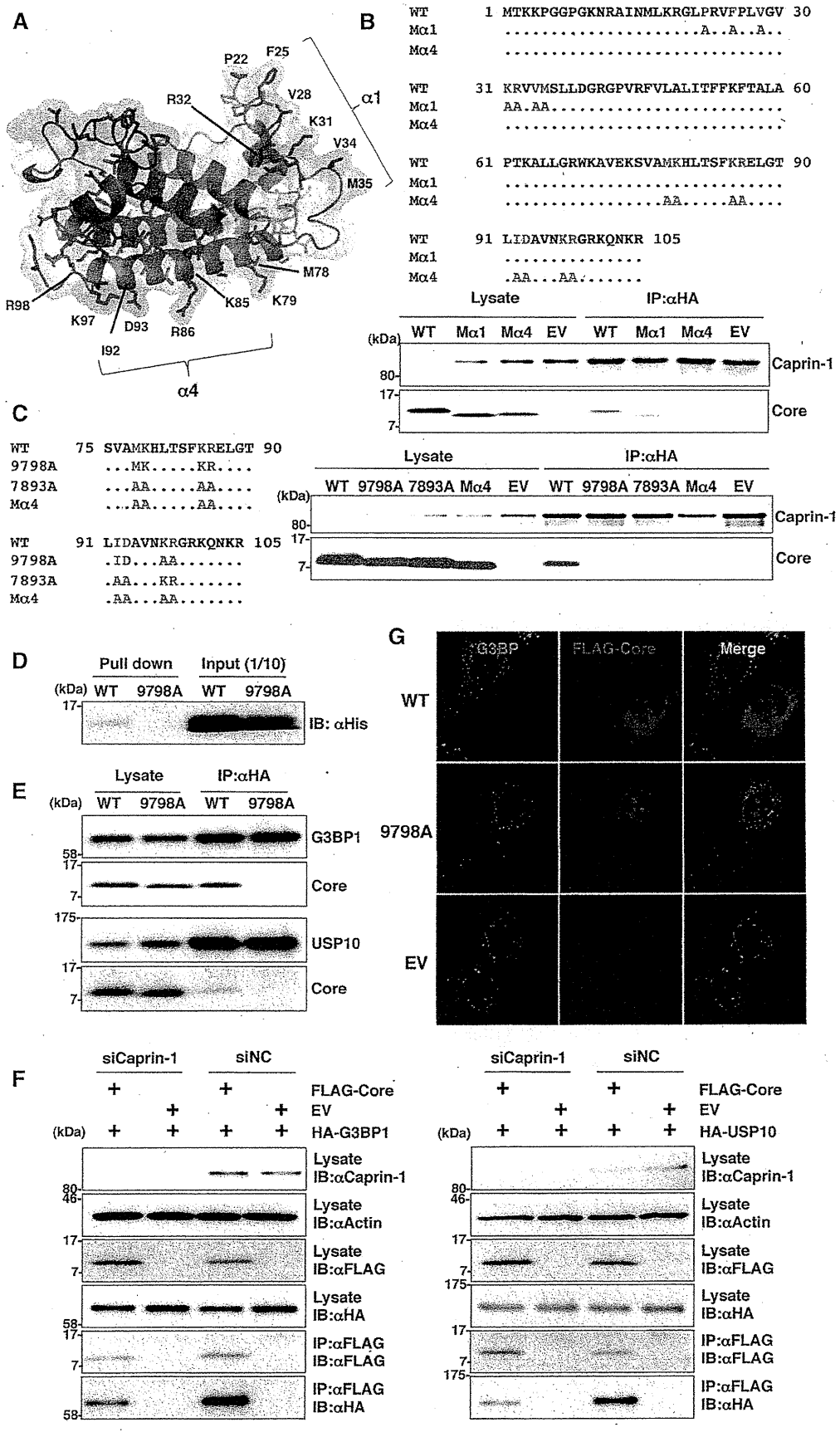
A
P22
F25
R32
V28
α1
K31
V34
M35
M78
R98
K97
D93
R86
K85
K79
I92
α4
B
WT 1 MTKKPGGPGKNRAINMLKRGLPRVFPLVGV 30
Mα1 .....A..A..A..
Mα4 .....
WT 31 KRVVMSLLDGRGPVRFVLALITFFKFTALA 60
Mα1 AA.AA.....
Mα4 .....
WT 61 PTKALLGRWKAVEKSVAMKHLTSFKRELGT 90
Mα1 .....
Mα4 .....AA.....AA....
WT 91 LIDAVNKRGRKQNKR 105
Mα1 .....
Mα4 .AA...AA.....
Lysate
IP:αHA
(kDa)
WT Mα1 Mα4 EV WT Mα1 Mα4 EV
80
17
7
Caprin-1
Core
C
WT 75 SVAMKHLTSFKRELGT 90
9798A ...MK.....KR....
7893A ...AA.....AA....
Mα4 ...AA.....AA....
WT 91 LIDAVNKRGRKQNKR 105
9798A .ID...AA.....
7893A .AA...KR.....
Mα4 .AA...AA.....
Lysate
IP:αHA
(kDa)
WT 9798A 7893A Mα4 EV WT 9798A 7893A Mα4 EV
80
17
7
Caprin-1
Core
D
Pull down
Input (1/10)
(kDa) WT 9798A WT 9798A
17
IB: αHis
E
Lysate
IP:αHA
(kDa) WT 9798A WT 9798A
58
G3BP1
17
7
Core
175
USP10
17
7
Core
G
G3BP
FLAG-Core
Merge
WT
9798A
EV
F
siCaprin-1
siNC
+ + FLAG-Core
+ + EV
(kDa) + + + + HA-G3BP1
Lysate IB:αCaprin-1
80
46
Lysate IB:αActin
17
7
Lysate IB:αFLAG
Lysate IB:αHA
58
17
7
IP:αFLAG IB:αFLAG
58
IP:αFLAG IB:αHA
siCaprin-1
siNC
+ + FLAG-Core
+ + EV
(kDa) + + + + HA-USP10
Lysate IB:αCaprin-1
80
46
Lysate IB:αActin
17
7
Lysate IB:αFLAG
175
Lysate IB:αHA
17
7
IP:αFLAG IB:αFLAG
175
IP:αFLAG IB:αHA

cipitation assay. As shown in Fig. 8C, double replacing both Lys^{97} and Arg^{98} with Ala (9798A) completely abrogated the interaction with Caprin-1. The importance of these two amino acids in the interaction with Caprin-1 was also confirmed by GST pulldown assay (Fig. 8D). These results indicate that Lys^{97} and Arg^{98} in the JEV core protein are crucial for the interaction with Caprin-1. Since G3BP has been reported to be one of the key molecules for SG formation and interacts with several SG component molecules including Caprin-1 and USP10 (28, 29), interactions of the core protein with SG components were examined by immunoprecipitation assay. The wild-type but not mutant 9798A core protein was associated with G3BP1 and USP10 (Fig. 8E). In addition, the knockdown of Caprin-1 weakened the interactions of core protein with G3BP1 or USP10 (Fig. 8F). These findings indicate that JEV core protein associates with several SG component molecules, such as G3BP1 and USP10, through the interaction with Caprin-1. Next, the role of the interaction between JEV core protein and Caprin-1 in the suppression of SG formation was examined by immunofluorescence analysis. Although the expression of the wild-type JEV core protein suppressed the SG formation induced by sodium arsenite treatment, as shown above, expression of the 9798A mutant did not (Fig. 8G), suggesting that the interaction of JEV core protein with Caprin-1 through Lys^{97} and Arg^{98} plays a crucial role in the inhibition of SG formation.

Interaction of the JEV core protein with Caprin-1 plays crucial roles not only in viral propagation *in vitro* but also in the pathogenesis in mice through the suppression of SG formation. To further examine the biological significance of the interaction between the JEV core protein and Caprin-1 in viral replication, we generated a mutant infectious cDNA clone (pMWJEAT/9798AA) of JEV encoding a mutant core protein deficient in the binding to Caprin-1 based on pMWJEAT. First, the cellular localization of the core protein in the 9798A mutant JEV-infected cells was examined by immunofluorescence analysis. The 9798A mutant core protein, as well as the wild-type core protein, was localized in the nucleus and the perinuclear region (Fig. 9A). However, the 9798A mutant core protein was not colocalized with Caprin-1, in contrast to the wild-type core protein. The sizes of infectious foci in Vero cells infected with the 9798A mutant were significantly smaller than those infected with the wild-type JEV (Fig. 9B). Furthermore, the infectious titers in C6/36 and Vero cells infected with the 9798A mutant were 6.1- and 12.6-fold lower than those infected with wild-type JEV at 48 h postinfection, respectively (Fig. 9C), suggesting that interaction of the JEV core protein with Caprin-1 plays crucial roles in the propagation of JEV in both insect and mammalian cells. Cells infected with the 9798A mutant induced SGs containing both G3BP and Caprin-1, in contrast to the accumulation of G3BP in the perinuclear region observed in those infected with the wild-type JEV (Fig. 9D). The numbers of foci in cells infected with the 9798A mutant were higher than those in cells infected with the wild-type JEV (Fig. 9E), indicating that the interaction of the JEV core protein with Caprin-1 is crucial for the suppression of SG formation. Finally, we examined the biological relevance of the interaction of JEV core protein with Caprin-1 in viral replication *in vivo*. Infectious particles were recovered from the cerebrums of ICR mice inoculated with wild-type JEV but not from those inoculated with the 9798A mutant (Fig. 9F). In addition, all 10 mice had died by 12 days postinoculation with the wild-type JEV, while only 1 mouse had died at day 10 postinoculation with the 9798A mutant (Fig. 9G). Collectively, these results suggest that the interaction of JEV core protein with Caprin-1 plays crucial roles not only in viral replication *in vitro* but also in pathogenesis in mice through the suppression of SG formation.

DISCUSSION

Viruses are obligatory intracellular parasites, and their life cycles rely on host cellular functions. Many viruses have evolved to inhibit SG formation and thereby evade the host translation shutoff mechanism and facilitate viral replication (6, 30), while some viruses co-opt molecules regulating SG formation for viral replication (11, 31). The vaccinia virus subverts SG components to generate aggregates containing G3BP, Caprin-1, eIF4G, eIF4E, and mRNA of the virus, but not of the host, in order to stimulate viral translation (11). Replication, translation, and assembly of transmissible gastroenteritis coronavirus, a member of the *Coronaviridae* family, are regulated by the interaction of polypyrimidine tract-binding protein and TIA-1 with viral RNA (31). HIV-1 utilizes Staufen1, which is a principal component of SG, in the viral RNA selection to form ribonucleoproteins (RNPs) through interaction with Gag protein, instead of SG translation silencing (8). In the case of flaviviruses, TIA-1 and TIAR bind to the 3′ untranslated region (UTR) of the negative-stranded RNA of WNV to facilitate viral replication (16), and G3BP1, Caprin-1, and USP10 interact with DENV RNA, although the biological significance of these interactions remains unknown (26). In this study, we have shown that JEV infection suppresses SG formation by the recruitment of several effector molecules promoting SG assembly, including G3BP and USP10, to the perinuclear region through the interaction of JEV core protein with Caprin-1. Furthermore, a mutant JEV carrying a core protein incapable of binding to

FIG 8 Lys^{97} and Arg^{98} in the JEV core protein are crucial residues for the interaction with Caprin-1. (A) Putative structural model of the core protein homodimer of JEV deduced from that of DENV obtained from the Protein Data Bank (accession number 1R6R) by using PyMOL software. The two α helices (α1 and α4) are indicated. (B) FLAG-Core mutants in which the hydrophobic amino acid residues in the α1 helix (Mα1) or α4 helix (Mα4) were replaced with alanine were coexpressed with HA-Caprin-1 in 293T cells, immunoprecipitated (IP) with anti-HA antibody, and examined by immunoblotting (IB) with anti-HA or anti-FLAG antibody. (C) FLAG-Core mutants in which the Met^{78}, Lys^{79}, Lys^{85}, Arg^{86}, Ile^{92}, and Asp^{93} (7893A) or Lys^{97} and Arg^{98} (9798A) in the α4 helix domain were replaced with alanine were coexpressed with HA-Caprin-1 in 293T cells and examined as described in panel B. (D) The His-tagged JEV core protein (WT or 9798A) was incubated with GST-fused Caprin-1 for 2 h at 4°C, and the precipitates obtained by GST pulldown assay were subjected to immunoblotting with anti-His antibody. (E) FLAG-Core (WT or 9798A) was coexpressed with HA-G3BP1 or HA-USP10 in 293T cells, immunoprecipitated with anti-HA antibody, and immunoblotted with anti-HA and anti-FLAG antibodies. (F) FLAG-JEV Core was coexpressed with HA-G3BP1 or HA-USP10 in 293T cells transfected with either siCaprin-1 or siNC at 72 h posttransfection, immunoprecipitated with anti-FLAG antibody, and immunoblotted with anti-HA and anti-FLAG antibodies. The cell lysates were also subjected to immunoblotting with anti-Caprin-1 and anti-β-actin antibodies to evaluate the knockdown efficiency of Caprin-1. (G) The cellular localizations of G3BP and FLAG-Core (WT or 9798A) were determined at 24 h posttransfection after treatment with 1.0 mM sodium arsenite for 30 min at 37°C by immunofluorescence analysis with mouse anti-G3BP MAb and rabbit anti-FLAG PAb, followed by AF488-conjugated anti-mouse IgG and AF594-conjugated anti-rabbit IgG, respectively. Cell nuclei were stained with DAPI (blue).

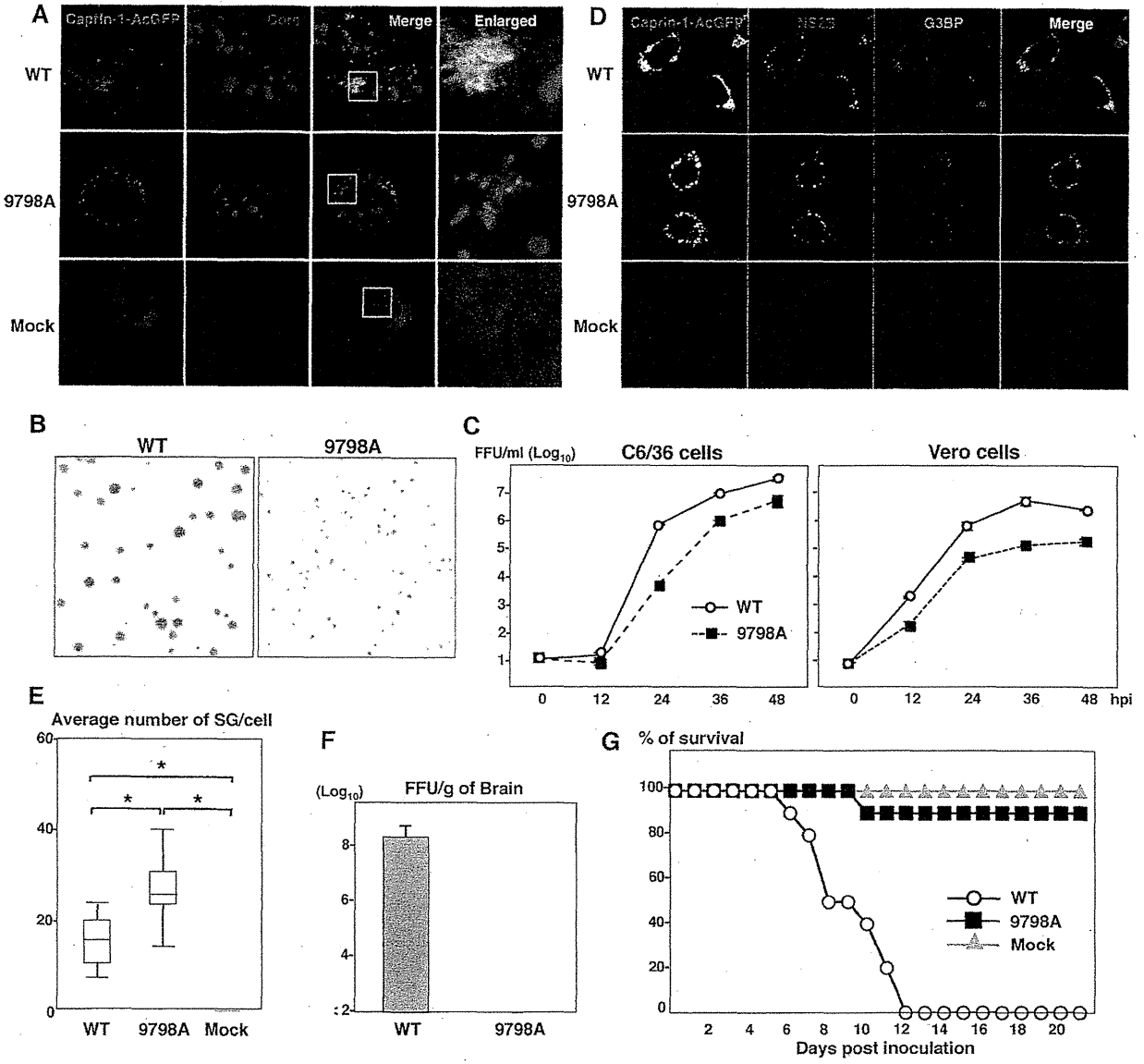

FIG 9 Interaction of JEV core protein with Caprin-1 plays crucial roles not only in viral replication *in vitro* but also in pathogenesis in mice through the suppression of SG formation. (A) Huh7/Caprin-1-AcGFP cells were infected with JEV (WT or 9798A mutant) at an MOI of 1.0, and the cellular localizations of Caprin-1-AcGFP and JEV core protein were determined at 24 h postinfection by immunofluorescence analysis with rabbit anti-core PAb and AF594-conjugated anti-rabbit IgG. Cell nuclei were stained with DAPI (blue). (B) Focus formation of JEV (WT or 9798A mutant) in Vero cells incubated in methylcellulose overlay medium at 48 h postinfection. The infectious foci were immunostained as described previously (20). (C) Growth kinetics of JEV (WT or 9798A mutant) in C6/36 and Vero cells infected at an MOI of 0.1. Infectious titers in the culture supernatants harvested at the indicated times were determined by focus-forming assays in Vero cells. Means of three experiments are indicated. (D) Huh7/Caprin-1-AcGFP cells were infected with either WT or 9798A at an MOI of 0.5, and cellular localizations of Caprin-1-AcGFP, G3BP (blue), and JEV NS2B (red) were determined at 24 h postinfection by immunofluorescence analysis with mouse anti-G3BP MAb and rabbit anti-NS2B PAb, followed by AF633-conjugated anti-mouse IgG and AF594-conjugated anti-rabbit IgG, respectively. (E) Numbers >of G3BP-positive foci in 30 cells prepared as described in panel D were counted. Lines, boxes, and error bars indicate the means, 25th to 75th percentiles, and 95th percentiles, respectively. The significance of differences between the means was determined by Student's *t* test. *, $P < 0.01$. (F) Infectious titers in the cerebrums of mice at 7 days postintraperitoneal inoculation with 5×10^4 FFU/100 μl of either WT or 9798A virus were determined in Vero cells. The means of titers in the homogenates of the cerebrums from three mice are indicated. The detection limit is 10^2 FFU/g of cerebrum. (G) Percentages of surviving mice ($n = 10$) after intraperitoneal inoculation with 5×10^4 FFU of either WT or 9798A virus. Mock, inoculation with DMEM.

Caprin-1 exhibited reduced replication *in vitro* and attenuated pathogenicity in mice.

G3BP is one of the key molecules involved in the SG aggregation process and self-oligomerizes in a phosphorylation-dependent manner to sequester mRNA in SGs (4). Therefore, G3BP knocked down cells (6) and G3BP knockout mouse embryonic fibroblast cells are deficient in the SG formation. In addition, G3BP sequestration inhibits SG formation in response to arsenite treatment (32). Caprin-1, known as RNA granule protein 105 or p137 (33), also participates in SG formation through phosphorylation of eIF2α (28) and is ubiquitously expressed in the cytoplasm. Caprin-1 regulates the transport and translation of mRNAs

of proteins involved in the synaptic plasticity in neurons (34) and cellular proliferation and migration in multiple cell types (28) through an interaction with G3BP. USP10, another SG-associated molecule, also interacts with G3BP and forms the G3BP/USP10 complex (29), suggesting that several SG-associated RBPs participate in the formation of a protein-protein network. In this study, the JEV core protein was shown to directly interact with Caprin-1, to sequester several key molecule complexes involved in SG formation to the perinuclear region in cells infected with JEV, and to facilitate viral propagation through the suppression of SG formation.

Flaviviruses replicate at a relatively low rate in comparison with most of the other positive-stranded RNA viruses, and thus rapid shutdown of host cellular protein synthesis would be deleterious for the viral life cycle. In cells infected with JEV, several SG components were colocalized with the core protein in the perinuclear region, while in those infected with WNV or DENV, SG components were accumulated in a replication complex composed of viral RNA and nonstructural proteins. In addition, the phosphorylation of eIF2α induced by arsenite was completely canceled by the infection with WNV or DENV, whereas the suppression of the phosphorylation was limited in JEV infection (15). Incorporation of the nascent viral RNA into the membranous structure induced by viral nonstructural proteins prevents PKR activation and inhibits SG formation in cells infected with WNV (17). In cells infected with hepatitis C virus (HCV), which belongs to the genus *Hepacivirus* in the family *Flaviviridae*, induction of SG formation was observed in the early stage of infection, in contrast to the inhibition of the arsenite-induced SG formation in the late stage (35). Several SG components, such as G3BP1, PABP1, and ataxin-2, were colocalized with HCV core protein around lipid droplets (35), and G3BP1 was also associated with the NS5B protein and the 5′ terminus of the minus-strand viral RNA (36) to mediate efficient viral replication. Collectively, these data suggest that flaviviruses have evolved to regulate cellular processes involved in SG formation through various strategies.

PKR is one of the interferon-stimulated genes and plays a crucial role in antiviral defense through phosphorylation of eIF2α, which leads to host translational shutoff (37, 38). In the early stage of flavivirus infection, both positive- and negative-stranded RNAs transcribe at low levels, while genomic RNA predominantly synthesizes in the late stage of infection (39). It was shown that activation of PKR was suppressed (40) or only induced in the late stage of WNV infection (41) and impaired by the expression of HCV NS5A (42–44). Very recently, JEV NS2A was shown to suppress PKR activation through inhibition of dimerization of PKR in the early stage but not in the late stage of infection (45). In this study, we have shown that JEV core protein interacts with Caprin-1 and inhibits SG formation downstream of the phosphorylation of eIF2α in the late stage of infection, suggesting that JEV has evolved to escape from host antiviral responses in the multiple stages of viral replication by using structural and nonstructural proteins.

The flavivirus core protein is a multifunctional protein involved in many aspects of the viral life cycle. In addition to the formation of viral nucleocapsid through the interaction with viral RNA (as a structural protein) (46), flavivirus core proteins interact with various host factors, such as B23 (47), Jab1 (48), hnRNP K (49), and hnRNP A2 (23), and regulate viral replication and/or modify the host cell environment (as a nonstructural protein). Although further investigations are needed to clarify the precise mechanisms underlying the circumvention of SG formation through the interaction of JEV core protein with Caprin-1, leading to efficient propagation *in vitro* and pathogenicity in mice, these findings could help not only to provide new insight into strategies by which viruses escape host stress responses but also to develop novel antiviral agents for flavivirus infection.

ACKNOWLEDGMENTS

We thank M. Tomiyama for secretarial assistance. We also thank K. Saito and T. Wakita for technical advice and the infectious clone of JEV, respectively.

This work was supported in part by grants-in-aid from the Ministry of Health, Labor, and Welfare, the Ministry of Education, Culture, Sports, Science, and Technology, and the Osaka University Global Center of Excellence Program. H. Katoh is a research fellow of the Japanese Society for the Promotion of Science.

REFERENCES

1. Nover L, Scharf KD, Neumann D. 1989. Cytoplasmic heat shock granules are formed from precursor particles and are associated with a specific set of mRNAs. Mol. Cell. Biol. 9:1298–1308.
2. Anderson P, Kedersha N. 2002. Stressful initiations. J. Cell Sci. 115:3227–3234.
3. Gilks N, Kedersha N, Ayodele M, Shen L, Stoecklin G, Dember LM, Anderson P. 2004. Stress granule assembly is mediated by prion-like aggregation of TIA-1. Mol. Biol. Cell 15:5383–5398.
4. Tourriere H, Chebli K, Zekri L, Courselaud B, Blanchard JM, Bertrand E, Tazi J. 2003. The RasGAP-associated endoribonuclease G3BP assembles stress granules. J. Cell Biol. 160:823–831.
5. Kedersha N, Cho MR, Li W, Yacono PW, Chen S, Gilks N, Golan DE, Anderson P. 2000. Dynamic shuttling of TIA-1 accompanies the recruitment of mRNA to mammalian stress granules. J. Cell Biol. 151:1257–1268.
6. White JP, Cardenas AM, Marissen WE, Lloyd RE. 2007. Inhibition of cytoplasmic mRNA stress granule formation by a viral proteinase. Cell Host Microbe 2:295–305.
7. Khaperskyy DA, Hatchette TF, McCormick C. 2012. Influenza A virus inhibits cytoplasmic stress granule formation. FASEB J. 26:1629–1639.
8. Abrahamyan LG, Chatel-Chaix L, Ajamian L, Milev MP, Monette A, Clement JF, Song R, Lehmann M, DesGroseillers L, Laughrea M, Boccaccio G, Mouland AJ. 2010. Novel Staufen1 ribonucleoproteins prevent formation of stress granules but favour encapsidation of HIV-1 genomic RNA. J. Cell Sci. 123:369–383.
9. McInerney GM, Kedersha NL, Kaufman RJ, Anderson P, Liljestrom P. 2005. Importance of eIF2α phosphorylation and stress granule assembly in alphavirus translation regulation. Mol. Biol. Cell 16:3753–3763.
10. Smith JA, Schmechel SC, Raghavan A, Abelson M, Reilly C, Katze MG, Kaufman RJ, Bohjanen PR, Schiff LA. 2006. Reovirus induces and benefits from an integrated cellular stress response. J. Virol. 80:2019–2033.
11. Katsafanas GC, Moss B. 2007. Colocalization of transcription and translation within cytoplasmic poxvirus factories coordinates viral expression and subjugates host functions. Cell Host Microbe 2:221–228.
12. Misra UK, Kalita J. 2010. Overview: Japanese encephalitis. Prog. Neurobiol. 91:108–120.
13. Sumiyoshi H, Mori C, Fuke I, Morita K, Kuhara S, Kondou J, Kikuchi Y, Nagamatu H, Igarashi A. 1987. Complete nucleotide sequence of the Japanese encephalitis virus genome RNA. Virology 161:497–510.
14. Murray CL, Jones CT, Rice CM. 2008. Architects of assembly: roles of *Flaviviridae* non-structural proteins in virion morphogenesis. Nat. Rev. Microbiol. 6:699–708.
15. Emara MM, Brinton MA. 2007. Interaction of TIA-1/TIAR with West Nile and dengue virus products in infected cells interferes with stress granule formation and processing body assembly. Proc. Natl. Acad. Sci. U. S. A. 104:9041–9046.
16. Li W, Li Y, Kedersha N, Anderson P, Emara M, Swiderek KM, Moreno GT, Brinton MA. 2002. Cell proteins TIA-1 and TIAR interact with the 3′ stem-loop of the West Nile virus complementary minus-strand RNA and facilitate virus replication. J. Virol. 76:11989–12000.
17. Courtney SC, Scherbik SV, Stockman BM, Brinton MA. 2012. West Nile

virus infections suppress early viral RNA synthesis and avoid inducing the cell stress granule response. J. Virol. 86:3647–3657.
18. Kambara H, Tani H, Mori Y, Abe T, Katoh H, Fukuhara T, Taguwa S, Moriishi K, Matsuura Y. 2011. Involvement of cyclophilin B in the replication of Japanese encephalitis virus. Virology 412:211–219.
19. Mori Y, Yamashita T, Tanaka Y, Tsuda Y, Abe T, Moriishi K, Matsuura Y. 2007. Processing of capsid protein by cathepsin L plays a crucial role in replication of Japanese encephalitis virus in neural and macrophage cells. J. Virol. 81:8477–8487.
20. Mori Y, Okabayashi T, Yamashita T, Zhao Z, Wakita T, Yasui K, Hasebe F, Tadano M, Konishi E, Moriishi K, Matsuura Y. 2005. Nuclear localization of Japanese encephalitis virus core protein enhances viral replication. J. Virol. 79:3448–3458.
21. Kambara H, Fukuhara T, Shiokawa M, Ono C, Ohara Y, Kamitani W, Matsuura Y. 2012. Establishment of a novel permissive cell line for the propagation of hepatitis C virus by expression of microRNA miR122. J. Virol. 86:1382–1393.
22. Zhao Z, Date T, Li Y, Kato T, Miyamoto M, Yasui K, Wakita T. 2005. Characterization of the E-138 (Glu/Lys) mutation in Japanese encephalitis virus by using a stable, full-length, infectious cDNA clone. J. Gen. Virol. 86:2209–2220.
23. Katoh H, Mori Y, Kambara H, Abe T, Fukuhara T, Morita E, Moriishi K, Kamitani W, Matsuura Y. 2011. Heterogeneous nuclear ribonucleoprotein A2 participates in the replication of Japanese encephalitis virus through an interaction with viral proteins and RNA. J. Virol. 85:10976–10988.
24. Hamamoto I, Nishimura Y, Okamoto T, Aizaki H, Liu M, Mori Y, Abe T, Suzuki T, Lai MM, Miyamura T, Moriishi K, Matsuura Y. 2005. Human VAP-B is involved in hepatitis C virus replication through interaction with NS5A and NS5B. J. Virol. 79:13473–13482.
25. Jones CT, Ma L, Burgner JW, Groesch TD, Post CB, Kuhn RJ. 2003. Flavivirus capsid is a dimeric alpha-helical protein. J. Virol. 77:7143–7149.
26. Ward AM, Bidet K, Yinglin A, Ler SG, Hogue K, Blackstock W, Gunaratne J, Garcia-Blanco MA. 2011. Quantitative mass spectrometry of DENV-2 RNA-interacting proteins reveals that the DEAD-box RNA helicase DDX6 binds the DB1 and DB2 3′ UTR structures. RNA Biol. 8:1173–1186.
27. Ma L, Jones CT, Groesch TD, Kuhn RJ, Post CB. 2004. Solution structure of dengue virus capsid protein reveals another fold. Proc. Natl. Acad. Sci. U. S. A. 101:3414–3419.
28. Solomon S, Xu Y, Wang B, David MD, Schubert P, Kennedy D, Schrader JW. 2007. Distinct structural features of Caprin-1 mediate its interaction with G3BP-1 and its induction of phosphorylation of eukaryotic translation initiation factor 2α, entry to cytoplasmic stress granules, and selective interaction with a subset of mRNAs. Mol. Cell. Biol. 27:2324–2342.
29. Soncini C, Berdo I, Draetta G. 2001. Ras-GAP SH3 domain binding protein (G3BP) is a modulator of USP10, a novel human ubiquitin specific protease. Oncogene 20:3869–3879.
30. Montero H, Rojas M, Arias CF, Lopez S. 2008. Rotavirus infection induces the phosphorylation of eIF2α but prevents the formation of stress granules. J. Virol. 82:1496–1504.
31. Sola I, Galan C, Mateos-Gomez PA, Palacio L, Zuniga S, Cruz JL, Almazan F, Enjuanes L. 2011. The polypyrimidine tract-binding protein affects coronavirus RNA accumulation levels and relocalizes viral RNAs to novel cytoplasmic domains different from replication-transcription sites. J. Virol. 85:5136–5149.
32. Hinton SD, Myers MP, Roggero VR, Allison LA, Tonks NK. 2010. The pseudophosphatase MK-STYX interacts with G3BP and decreases stress granule formation. Biochem. J. 427:349–357.
33. Grill B, Wilson GM, Zhang KX, Wang B, Doyonnas R, Quadroni M, Schrader JW. 2004. Activation/division of lymphocytes results in increased levels of cytoplasmic activation/proliferation-associated protein-1: prototype of a new family of proteins. J. Immunol. 172:2389–2400.
34. Shiina N, Shinkura K, Tokunaga M. 2005. A novel RNA-binding protein in neuronal RNA granules: regulatory machinery for local translation. J. Neurosci. 25:4420–4434.
35. Ariumi Y, Kuroki M, Kushima Y, Osugi K, Hijikata M, Maki M, Ikeda M, Kato N. 2011. Hepatitis C virus hijacks P-body and stress granule components around lipid droplets. J. Virol. 85:6882–6892.
36. Yi Z, Pan T, Wu X, Song W, Wang S, Xu Y, Rice CM, Macdonald MR, Yuan Z. 2011. Hepatitis C virus co-opts Ras-GTPase-activating protein-binding protein 1 for its genome replication. J. Virol. 85:6996–7004.
37. Gale M, Jr, Katze MG. 1998. Molecular mechanisms of interferon resistance mediated by viral-directed inhibition of PKR, the interferon-induced protein kinase. Pharmacol. Ther. 78:29–46.
38. Pindel A, Sadler A. 2011. The role of protein kinase R in the interferon response. J. Interferon Cytokine Res. 31:59–70.
39. Chu PW, Westaway EG. 1985. Replication strategy of Kunjin virus: evidence for recycling role of replicative form RNA as template in semiconservative and asymmetric replication. Virology 140:68–79.
40. Elbahesh H, Scherbik SV, Brinton MA. 2011. West Nile virus infection does not induce PKR activation in rodent cells. Virology 421:51–60.
41. Samuel MA, Whitby K, Keller BC, Marri A, Barchet W, Williams BR, Silverman RH, Gale M, Jr, Diamond MS. 2006. PKR and RNase L contribute to protection against lethal West Nile Virus infection by controlling early viral spread in the periphery and replication in neurons. J. Virol. 80:7009–7019.
42. Gale M, Jr, Blakely CM, Kwieciszewski B, Tan SL, Dossett M, Tang NM, Korth MJ, Polyak SJ, Gretch DR, Katze MG. 1998. Control of PKR protein kinase by hepatitis C virus nonstructural 5A protein: molecular mechanisms of kinase regulation. Mol. Cell. Biol. 18:5208–5218.
43. Gale MJ, Jr, Korth MJ, Tang NM, Tan SL, Hopkins DA, Dever TE, Polyak SJ, Gretch DR, Katze MG. 1997. Evidence that hepatitis C virus resistance to interferon is mediated through repression of the PKR protein kinase by the nonstructural 5A protein. Virology 230:217–227.
44. He Y, Tan SL, Tareen SU, Vijaysri S, Langland JO, Jacobs BL, Katze MG. 2001. Regulation of mRNA translation and cellular signaling by hepatitis C virus nonstructural protein NS5A. J. Virol. 75:5090–5098.
45. Tu YC, Yu CY, Liang JJ, Lin E, Liao CL, Lin YL. 2012. Blocking dsRNA-activated protein kinase PKR by Japanese encephalitis virus nonstructural protein 2A. J. Virol. 86:10347–10358.
46. Khromykh AA, Westaway EG. 1996. RNA binding properties of core protein of the flavivirus Kunjin. Arch. Virol. 141:685–699.
47. Tsuda Y, Mori Y, Abe T, Yamashita T, Okamoto T, Ichimura T, Moriishi K, Matsuura Y. 2006. Nucleolar protein B23 interacts with Japanese encephalitis virus core protein and participates in viral replication. Microbiol. Immunol. 50:225–234.
48. Oh W, Yang MR, Lee EW, Park KM, Pyo S, Yang JS, Lee HW, Song J. 2006. Jab1 mediates cytoplasmic localization and degradation of West Nile virus capsid protein. J. Biol. Chem. 281:30166–30174.
49. Chang CJ, Luh HW, Wang SH, Lin HJ, Lee SC, Hu ST. 2001. The heterogeneous nuclear ribonucleoprotein K (hnRNP K) interacts with dengue virus core protein. DNA Cell Biol. 20:569–577.

HEPATOLOGY
Official Journal of the American Association for the Study of Liver Diseases

Human Blood Dendritic Cell Antigen 3 (BDCA3)$^+$ Dendritic Cells Are a Potent Producer of Interferon-λ in Response to Hepatitis C Virus

Sachiyo Yoshio,[1] Tatsuya Kanto,[1] Shoko Kuroda,[1] Tokuhiro Matsubara,[1] Koyo Higashitani,[1] Naruyasu Kakita,[1] Hisashi Ishida,[1] Naoki Hiramatsu,[1] Hiroaki Nagano,[2] Masaya Sugiyama,[3] Kazumoto Murata,[3] Takasuke Fukuhara,[4] Yoshiharu Matsuura,[4] Norio Hayashi,[5] Masashi Mizokami,[3] and Tetsuo Takehara[1]

The polymorphisms in the interleukin (*IL*)-*28B* (interferon-lambda [IFN]-λ3) gene are strongly associated with the efficacy of hepatitis C virus (HCV) clearance. Dendritic cells (DCs) sense HCV and produce IFNs, thereby playing some cooperative roles with HCV-infected hepatocytes in the induction of interferon-stimulated genes (ISGs). Blood dendritic cell antigen 3 (BDCA3)$^+$ DCs were discovered as a producer of IFN-λ upon Toll-like receptor 3 (TLR3) stimulation. We thus aimed to clarify the roles of BDCA3$^+$ DCs in anti-HCV innate immunity. Seventy healthy subjects and 20 patients with liver tumors were enrolled. BDCA3$^+$ DCs, in comparison with plasmacytoid DCs and myeloid DCs, were stimulated with TLR agonists, cell-cultured HCV (HCVcc), or Huh7.5.1 cells transfected with HCV/JFH-1. BDCA3$^+$ DCs were treated with anti-CD81 antibody, inhibitors of endosome acidification, TIR-domain-containing adapter-inducing interferon-β (TRIF)-specific inhibitor, or ultraviolet-irradiated HCVcc. The amounts of IL-29/IFN-λ1, IL-28A/IFN-λ2, and IL-28B were quantified by subtype-specific enzyme-linked immunosorbent assay (ELISA). The frequency of BDCA3$^+$ DCs in peripheral blood mononuclear cell (PBMC) was extremely low but higher in the liver. BDCA3$^+$ DCs recovered from PBMC or the liver released large amounts of IFN-λs, when stimulated with HCVcc or HCV-transfected Huh7.5.1. BDCA3$^+$ DCs were able to induce ISGs in the coexisting JFH-1-positive Huh7.5.1 cells. The treatments of BDCA3$^+$ DCs with anti-CD81 antibody, cloroquine, or bafilomycin A1 reduced HCVcc-induced IL-28B release, whereas BDCA3$^+$ DCs comparably produced IL-28B upon replication-defective HCVcc. The TRIF-specific inhibitor reduced IL-28B release from HCVcc-stimulated BDCA3$^+$ DCs. In response to HCVcc or JFH-1-Huh7.5.1, BDCA3$^+$ DCs in healthy subjects with IL-28B major (rs8099917, TT) released more IL-28B than those with IL-28B minor genotype (TG). *Conclusion*: Human BDCA3$^+$ DCs, having a tendency to accumulate in the liver, recognize HCV in a CD81-, endosome-, and TRIF-dependent manner and produce substantial amounts of IL-28B/IFN-λ3, the ability of which is superior in subjects with IL-28B major genotype. (HEPATOLOGY 2013;57:1705-1715)

Hepatitis C virus (HCV) infection is one of the most serious health problems in the world. More than 170 million people are chronically infected with HCV and are at high risk of developing liver cirrhosis and hepatocellular carcinoma. Genome-wide association studies have successfully identified the genetic polymorphisms (single nucleotide polymorphisms, SNPs) upstream of the promoter region of the

Abbreviations: Ab, antibody; HCV, hepatitis C virus; HCVcc, cell-cultured hepatitis C virus; HSV, herpes simplex virus; IHL, intrahepatic lymphocyte; INF-λ, interferon-lambda; IRF, interferon regulatory factor; ISGs, interferon-stimulated genes; JEV, Japanese encephalitis virus; Lin, lineage; mDC, myeloid DC; MOI, multiplicity of infection; PBMC, peripheral blood mononuclear cell; pDC, plasmacytoid DC; Poly IC, polyinosine-polycytidylic acid; RIG-I, retinoic acid-inducible gene-I; SNPs, single nucleotide polymorphisms; TLR, Toll-like receptor; TRIF, TIR-domain-containing adapter-inducing interferon-β.

From the [1]Department of Gastroenterology and Hepatology, Osaka University Graduate School of Medicine, Osaka, Japan; [2]Department of Surgery, Osaka University Graduate School of Medicine, Osaka, Japan; [3]Research Center for Hepatitis and Immunology, National Center for Global Health and Medicine, Ichikawa, Japan; [4]Department of Molecular Virology, Research Institute for Microbial Diseases, Osaka University, Osaka, Japan; [5]Kansai Rosai Hospital, Hyogo, Japan.

Received July 2, 2012; accepted November 13, 2012.

Supported in part by a Grant-In-Aid for Scientific Research from the Ministry of Education, Culture, Sports, Science, and Technology, Japan and a Grant-In-Aid from the Ministry of Health, Labor, and Welfare of Japan.

interleukin (IL)-28B / interferon-lambda 3 (IFN-λ3) gene, which are strongly associated with the efficacy of pegylated interferon-α (PEG-IFN-α) and ribavirin therapy or spontaneous HCV clearance.[1-4]

IFN-λs, or type III IFNs, comprise a family of highly homologous molecules consisting of IFN-λ1 (IL-29), IFN-λ2 (IL-28A), and IFN-λ3 (IL-28B). In clear contrast to type I IFNs, they are released from relatively restricted types of cells, such as hepatocytes, intestinal epithelial cells, or dendritic cells (DCs). Also, the cells that express heterodimeric IFN-λ receptors (IFN-λR1 and IL-10R2) are restricted to cells of epithelial origin, hepatocytes, or DCs.[5] Such limited profiles of cells expressing IFN-λs and their receptors define the biological uniqueness of IFN-λs. It has been shown that IFN-λs convey anti-HCV activity by inducing various interferon-stimulated genes (ISGs),[5] the profiles of which were overlapped but others were distinct from those induced by IFN-α/β. Some investigators showed that the expression of IL-28 in PBMC was higher in subjects with IL-28B major than those with minor; however, the levels of IL-28 transcripts in liver tissue were comparable regardless of IL-28B genotype.[2,6]

At the primary exposure to hosts, HCV maintains high replicative levels in the infected liver, resulting in the induction of IFNs and ISGs. In a case of successful HCV eradication, it is postulated that IFN-α/β and IFN-λ cooperatively induce antiviral ISGs in HCV-infected hepatocytes. It is of particular interest that, in primary human hepatocytes or chimpanzee liver, IFN-λs, but not type I IFNs, are primarily induced after HCV inoculation, the degree of which is closely correlated with the levels of ISGs.[7] These results suggest that hepatic IFN-λ could be a principal driver of ISG induction in response to HCV infection. Nevertheless, the possibility remains that DCs, as a prominent IFN producer in the liver, play significant roles in inducing hepatic ISGs and thereby suppressing HCV replication.

DCs, as immune sentinels, sense specific genomic and/or structural components of pathogens with various pattern recognition receptors and eventually release IFNs and inflammatory cytokines.[8] In general, DCs migrate to the organ where inflammation or cellular apoptosis occurs and alter their function in order to alleviate or exacerbate the disease conditions. Therefore, the phenotypes and/or capacity of liver DCs are deemed to be influenced in the inflamed liver. In humans, the existence of phenotypically and functionally distinct DC subsets has been reported: myeloid DC (mDC) and plasmacytoid DC (pDC).[9] Myeloid DCs predominantly produce IL-12 or tumor necrosis factor alpha (TNF-α) following proinflammatory stimuli, while pDCs release considerable amounts of type I IFNs upon virus infection.[9] The other type of mDCs, mDC2 or BDCA3$^+$(CD141) DCs, have been drawing much attention recently, since human BDCA3$^+$ DCs are reported to be a counterpart of murine CD8a$^+$ DCs.[10] Of particular interest is the report that BDCA3$^+$ DCs have a potent capacity of releasing IFN-λ in response to Toll-like receptor 3 (TLR3) agonist.[11] However, it is still largely unknown whether human BDCA3$^+$ DCs are able to respond to HCV.

Taking these reports into consideration, we hypothesized that human BDCA3$^+$ DCs, as a producer of IFN-λs, have crucial roles in anti-HCV innate immunity. We thus tried to clarify the potential of BDCA3$^+$ DCs in producing type III IFNs by using cell-cultured HCV (HCVcc) or hepatoma cells harboring HCV as stimuli. Our findings show that BDCA3$^+$ DCs are quite a unique DC subset, characterized by a potent and specialized ability to secrete IFN-λs in response to HCV. The ability of BDCA3$^+$ DCs to release IL-28B upon HCV is superior in subjects with IL-28B major (rs8099917, TT) to those with minor (TG or GG) genotype, suggesting that BDCA3$^+$ DCs are one of the key players in IFN-λ-mediated innate immunity.

Patients and Methods

Subjects. This study enrolled 70 healthy volunteers (male/female: 61/9) (age: mean ± standard deviation [SD], 37.3 ± 7.8 years) and 20 patients who underwent surgical resection of liver tumors at Osaka University Hospital (Supporting Table 1). The study was approved by the Ethical Committee of Osaka University Graduate School of Medicine. Written informed consent was obtained from all of them. All healthy volunteers were negative for HCV, hepatitis B virus (HBV), and human immunodeficiency virus (HIV) and had no apparent history of liver, autoimmune, or malignant diseases.

Address reprint requests to: Tatsuya Kanto, M.D., Ph.D., Department of Gastroenterology and Hepatology, Osaka University Graduate School of Medicine, 2-2 Yamadaoka, Suita, 565-0871 Japan. E-mail: kantot@gh.med.osaka-u.ac.jp; fax: +81-6-6879-3629.

View this article online at wileyonlinelibrary.com.

DOI 10.1002/hep.26182

Potential conflict of interest: Nothing to report.

Additional Supporting Information may be found in the online version of this article.

Reagents. The specifications of all antibodies used for FACS or cell sorting TLR-specific synthetic agonists, pharmacological reagents, and inhibitory peptides are listed in the Supporting Materials.

Separation of DCs from PBMC or Intrahepatic Lymphocytes. We collected 400 mL of blood from each healthy volunteer and processed them for PBMCs. Noncancerous liver tissues were obtained from patients who underwent resection of liver tumors (Supporting Table 1). For the collection of intrahepatic lymphocytes (IHLs), liver tissues were washed thoroughly with phosphate-buffered saline to remove the peripheral blood adhering to the tissue and ground gently. After Lin-negative ($CD3^-$, $CD14^-$, $CD19^-$, and $CD56^-$) cells were obtained by the MACS system, each DC subset with the defined phenotype was sorted separately under FACS Aria (BD). The purity was more than 98%, as assessed by FACS Canto II (BD). Sorted DCs were cultured at 2.5×10^4/well on 96-well culture plates.

Immunofluorescence Staining of Human Liver Tissue. Tissue specimens were obtained from surgical resections of noncancerous liver from the patients as described above. Briefly, the 5-mm sections were incubated with the following antibodies: mouse biotinylated antihuman BDCA3 antibody (Miltenyi-Biotec), and mouse antihuman CLEC9A antibody (Biolegend) and subsequently with secondary goat antirabbit Alexa Fluor488 or goat antimouse Alexa Fluor594 (Invitrogen, Molecular Probes) antibodies. Cell nuclei were counterstained with Dapi-Fluoromount-GTM (Southern Biotech, Birmingham, AL). The stained tissues were analyzed by fluorescence microscopy (Model BZ-9000; Keyence, Osaka, Japan).

Cells and Viruses. The *in vitro* transcribed RNA of the JFH-1 strain of HCV was introduced into FT3-7 cells[12] or Huh7.5.1 cells. The stocks of HCVcc were generated by concentration of the medium from JFH-1-infected FT3-7 cells. The virus titers were determined by focus forming assay.[13] The control medium was generated by concentration of the medium from HCV-uninfected FT3-7 cells. Infectious JEVs were generated from the expression plasmid (pMWJEATG1) as reported.[14] HSV (KOS) was a generous gift from Dr. K. Ueda (Osaka University). Huh7.5.1 cells transduced with HCV JFH-1 strain was used for the coculture with DCs. The transcripts of ISGs in Huh7.5.1 were examined by reverse-transcription polymerase chain reaction (RT-PCR) methods using gene-specific primers and probes (Applied Biosystems, Foster City, CA).

Secretion Assays. IL-28B/IFN-λ3 was quantified by a newly developed chemiluminescence enzyme immunoassay (CLEIA) system.[15] IL-29/IFN-λ1, IL-28A/IFN-λ2, and IFN-β were assayed by commercially available enzyme-linked immunosorbent assay (ELISA) kits (eBioscience, R&D, and PBL, respectively). IFN-α was measured by cytometric beads array kits (BD) according to the manufacturer's instructions.

Statistical Analysis. The differences between two groups were assessed by the Mann-Whitney nonparametric *U* test. Multiple comparisons between more than two groups were analyzed by the Kruskal-Wallis nonparametric test. Paired *t* tests were used to compare differences in paired samples. All the analyses were performed using GraphPad Prism software (San Diego, CA).

Results

Human BDCA3$^+$ DCs Are Phenotypically Distinct from pDCs and mDCs. We defined $BDCA3^+$ DCs as $Lin^-HLA\text{-}DR^+BDCA3^{high+}$ cells (Fig. 1A, left, middle), and pDCs and mDCs by the patterns of CD11c and CD123 expressions (Fig. 1A, right). The level of CD86 on pDCs or mDCs is comparatively higher than those on $BDCA3^+$ DCs (Fig. 1B). The expression of CD81 is higher on $BDCA3^+$ DCs than on pDCs and mDCs (Fig. 1B, Supporting Fig. S1). CLEC9A, a member of C-type lectin, is expressed specifically on $BDCA3^+$ DCs as reported elsewhere,[16] but not on pDCs and mDCs (Fig. 1B).

Liver BDCA3$^+$ DCs Are More Mature than the Counterparts in the Periphery. $BDCA3^+$ DCs in infiltrated hepatic lymphocytes (IHLs) are all positive for CLEC9A, but liver pDCs or mDCs are not (data not shown). The levels of CD40, CD80, CD83, and CD86 on liver $BDCA3^+$ DCs are higher than those on the peripheral counterparts, suggesting that $BDCA3^+$ DCs are more mature in the liver compared to those in the periphery (Fig. 1C).

In order to confirm that $BDCA3^+$ DCs are localized in the liver, we stained the cells with immunofluorescence antibodies (Abs) in noncancerous liver tissues. Liver $BDCA3^+$ DCs were defined as $BDCA3^+$ $CLEC9A^+$ cells (Fig. 1D). Most of the cells were found near the vascular compartment or in sinusoid or the space of Disse of the liver tissue.

BDCA3$^+$ DCs Are Scarce in PBMCs but More Abundant in the Liver. The percentages of $BDCA3^+$ DCs in PBMCs were much lower than those of the other DC subsets ($BDCA3^+$ DCs, pDCs and mDCs, mean $\pm$ SD [%], 0.054 $\pm$ 0.044, 0.27 $\pm$ 0.21 and 1.30 $\pm$ 0.65) (Fig. 2A). The percentages of $BDCA3^+$ DCs in IHLs were lower than those of the others ($BDCA3^+$ DCs, pDCs, and mDCs, mean $\pm$ SD [%],

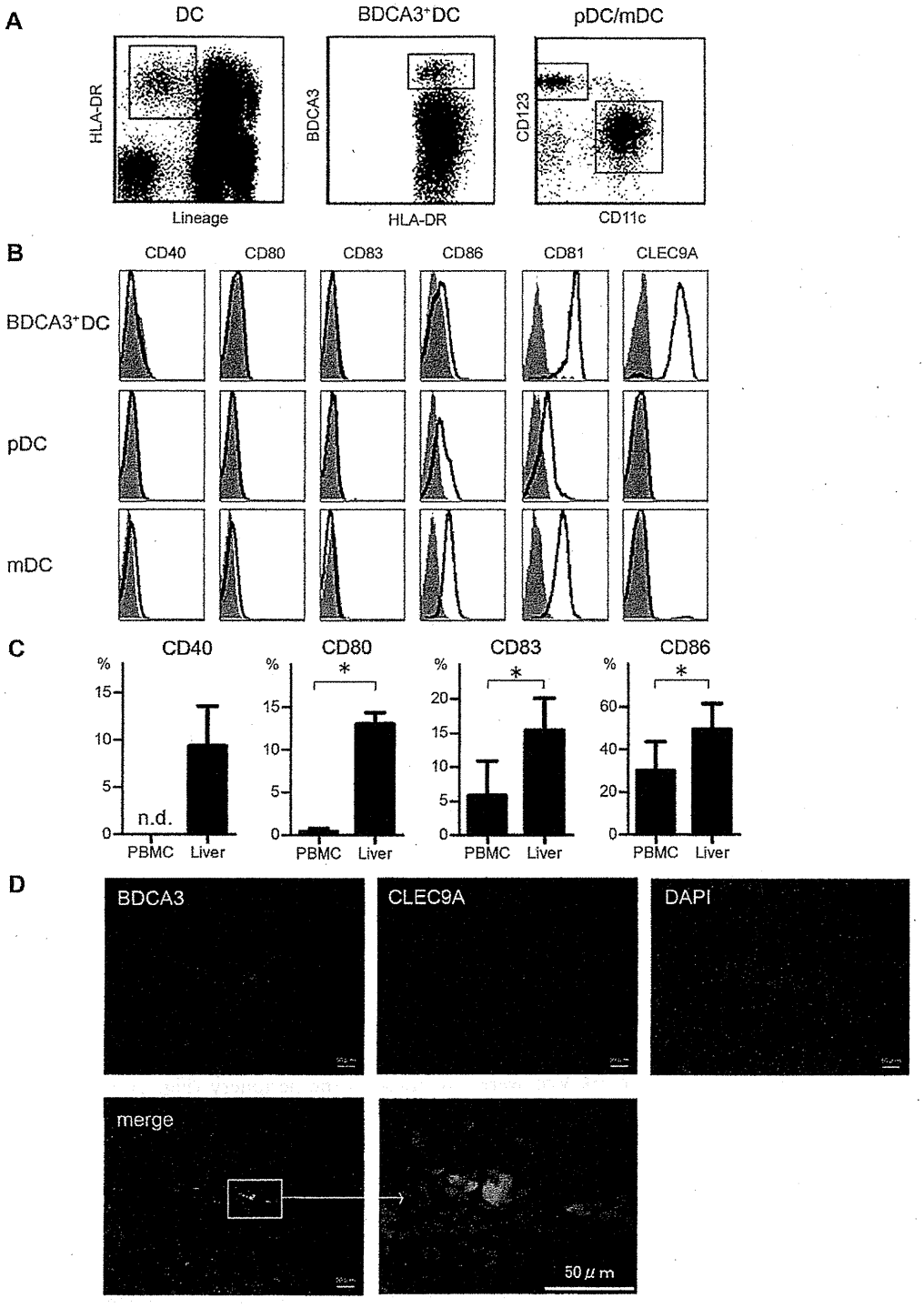

Fig. 1. Identification and phenotypic analyses of peripheral blood and intrahepatic BDCA3$^+$ DCs. (A) We defined BDCA3$^+$ DCs as Lineage$^-$HLA-DR$^+$BDCA3^{high+} cells (middle), pDCs as Lineage$^-$HLA-DR$^+$CD11c$^-$CD123^{high+} cells, and mDCs as Lineage$^-$HLA-DR$^+$CD11c$^+$CD123^{low+} cells (right). (B) The expressions of CD40, CD80, CD83, CD86, CD81, and CLEC9A on each DC subset in peripheral blood are shown. Representative results of five donors are shown in the histograms. Filled gray histograms depict data with isotype Abs, and open black ones are those with specific Abs. (C) The expressions of costimulatory molecules on BDCA3$^+$ DCs were compared between in PBMCs and in the liver. The results are shown as the percentage of positive cells. Results are the mean ± SEM from four independent experiments. *$P < 0.05$ by paired t test. (D) The staining for BDCA3 (green), CLEC9A (red) identifies BDCA3$^+$ DCs (merge, BDCA3$^+$CLEC9A$^+$) in human liver tissues. Representative results of the noncancerous liver samples are shown. BDCA, blood dendritic cell antigen; pDC, plasmacytoid DC; mDC, myeloid DC; CLEC9A, C-type lectin 9A.

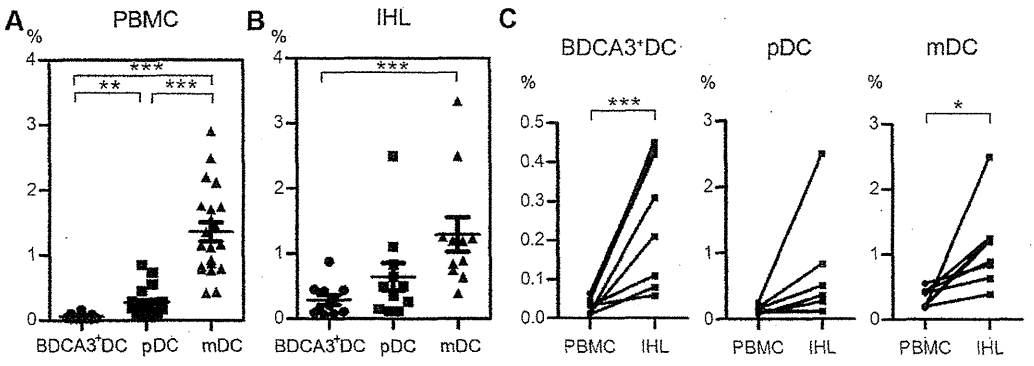

Fig. 2. Analysis of frequency of DC subsets in the peripheral blood and in the liver. Frequencies of BDCA3$^+$ DCs, pDCs, and mDCs in PBMCs (21 healthy subjects) (A) or in the intrahepatic lymphocytes (IHLs) (11 patients who had undergone surgical resection of tumors) (B) are shown. Horizontal bars depict the mean ± SD. $^{**}P < 0.005$; $^{***}P < 0.0005$ by Kruskal-Wallis test. (C) The paired comparisons of the frequencies of DC subsets between in PBMCs and in IHLs. the results of eight patients whose PBMCs and IHLs were obtained simultaneously are shown. $^{*}P < 0.05$; $^{***}P < 0.0005$ by paired *t* test. IHLs, intrahepatic lymphocytes; pDC and mDC, see Fig. 1.

0.29 ± 0.25, 0.65 ± 0.69 and 1.2 ± 0.94) (Fig. 2B). The percentages of BDCA3$^+$ DCs in the IHLs were significantly higher than those in PBMCs from relevant donors (Fig. 2C). Such relative abundance of BDCA3$^+$ DCs in the liver over that in the periphery was observed regardless of the etiology of the liver disease (Supporting Table 1).

BDCA3$^+$ DCs Produce a Large Amount of IFN-λs upon Poly IC Stimulation. We compared DC subsets for their abilities to produce IL-29/IFN-λ1, IL-28A/IFN-λ2, IL-28B/IFN-λ3, IFN-β, and IFN-α in response to TLR agonists. Approximately 4.0×10^4 of BDCA3$^+$ DCs were recoverable from 400 mL of donated blood from healthy volunteers. We fixed the number of DCs at 2.5×10^4 cells/100 mL for comparison in the following experiments.

BDCA3$^+$ DCs have been reported to express mRNA for TLR1, 2, 3, 6, 8, and 10.[17] First, we quantified IL-28B/IFN-λ3 as a representative for IFN-λs after stimulation of BDCA3$^+$ DCs with relevant TLR agonists. We confirmed that BDCA3$^+$ DCs released IL-28B robustly in response to TLR3 agonist/poly IC but not to other TLR agonists (Fig. S2). In contrast, pDCs produced IL-28B in response to TLR9 agonist/CpG but much lesser to other agonists (Fig. S2). Next, we compared the capabilities of DCs inducing IFN-λs and IFN-β genes in response to relevant TLR agonists. BDCA3$^+$ DCs expressed extremely high levels of IL-29, IL-28A, and IL-28B transcripts compared to other DCs, whereas pDCs induced a higher level of IFN-β than other DCs (Fig. S3A).

Similar results were obtained with the protein levels of IFN-λs, IFN-β, and IFN-α released from DC subsets stimulated with TLR agonists. BDCA3$^+$ DCs produce significantly higher levels of IL-29, IL-28B, and IL-28A than the other DC subsets. In clear contrast, pDCs release a significantly larger amount of IFN-β and IFN-α than BDCA3$^+$ DCs or mDCs (Fig. 3A, Fig. S3B). As for the relationship among the quantity of IFN-λ subtypes from poly IC-stimulated BDCA3$^+$ DCs, the levels of IL-29/IFN-λ1 and IL-28B/IFN-λ3 were positively correlated ($R^2 = 0.76$, $P < 0.05$), and those of IL-28A/IFN-λ2 and IL-28B/IFN-λ3 were positively correlated as well ($R^2 = 0.84$, $P < 0.0005$), respectively (Fig. S3C). These results show that the transcription and translation machineries of IFN-λs may be overlapped among IFN-λ subtypes in BDCA3$^+$ DCs upon poly IC stimulation.

Liver BDCA3$^+$ DCs sorted from IHLs possess the ability to produce IL-28B in response to poly IC (Fig. 3B), showing that they are comparably functional. In response to poly IC, BDCA3$^+$ DCs were capable of producing inflammatory cytokines as well, such as TNF-α, IL-6, and IL-12p70 (Fig. S4A). By using Huh7 cells harboring HCV subgenomic replicons (HCV-N, genotype 1b), we confirmed that the supernatants from poly IC-stimulated BDCA3$^+$ DCs suppressed HCV replication in an IL-28B concentration-dependent manner (Fig. S4B). Therefore, poly IC-stimulated BDCA3$^+$ DCs are capable of producing biologically active substances suppressing HCV replication, some part of which may be mediated by IFN-λs.

BDCA3$^+$ DCs Produce IL-28B upon HCVcc or HCV/JFH-1-Transfected Huh7.5.1 Cells. We stimulated freshly isolated BDCA3$^+$ DCs, pDCs and mDCs with infectious viruses, such as HCVcc, Japanese encephalitis virus (JEV), and herpes simplex virus (HSV). In preliminary experiments, we confirmed that HCVcc stimulated BDCA3$^+$ DCs to release IL-28B in a dose-dependent manner (Fig. S5). BDCA3$^+$ DCs

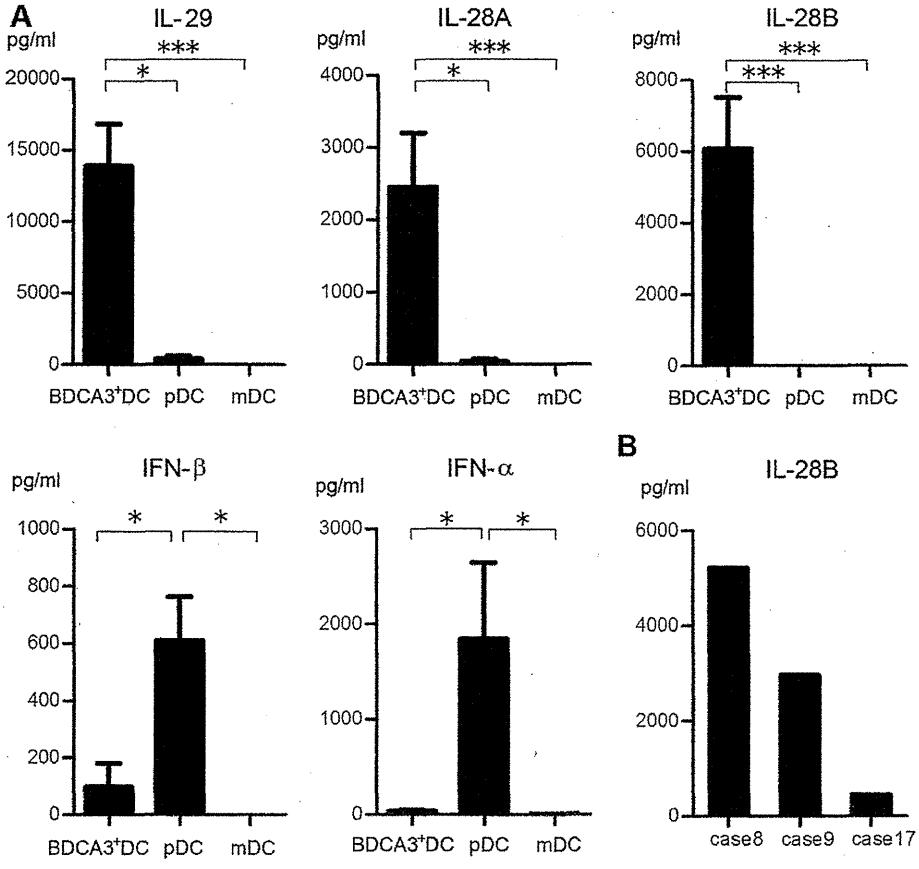

Fig. 3. BDCA3$^+$ DCs recovered from peripheral blood or intrahepatic lymphocytes produce large amounts of IL-29/IFN-λ1, IL-28A/IFN-λ2, and IL-28B/IFN-λ3 in response to poly IC. (A) BDCA3$^+$ DCs and mDCs were cultured at 2.5×10^4 cells with 25 mg/mL poly IC, and pDCs were with 5 mM CPG for 24 hours. The supernatants were examined for IL-29, IL-28A, IL-28B, IFN-β and IFN-α. Results are shown as mean $\pm$ SEM from 15 experiments. $^*P < 0.05$; $^{***}P < 0.0005$ by Kruskal-Wallis test. (B) For the IL-28B production, BDCA3$^+$ DCs in intrahepatic lymphocytes were cultured at 2.5×10^4 cells with 25 mg/mL poly IC for 24 hours. The samples of cases 8 and 9 were obtained from patients with non-B, non-C liver disease and that of case 17 was from an HCV-infected patient (Supporting Table 1).

produced a large amount of IL-28B upon exposure to HCVcc and released a lower amount of IFN-α upon HCVcc or HSV (Fig. 4A). In contrast, pDCs produced a large amount of IFN-α in response to HCVcc and HSV and a much lower level of IL-28B upon HCVcc (Fig. S6). In mDCs, IL-28B and IFN-α were not detectable with any of these viruses (data not shown).

BDCA3$^+$ DCs produced significantly higher levels of IL-28B than the other DCs upon HCVcc stimulation (Fig. 4B). By contrast, HCVcc-stimulated pDCs released significantly larger amounts of IFN-β and IFN-α than the other subsets (Fig. 4B). Liver BDCA3$^+$ DCs were capable of producing IL-28B in response to HCVcc (Fig. 4C). These results show that, upon HCVcc stimulation, BDCA3$^+$ DCs produce more IFN-λs and pDCs release more IFN-β and IFN-α than the other DC subsets, respectively. Taking a clinical impact of IL-28B genotypes on HCV eradication into consideration, we focused on IL-28B/IFN-λ3 as a representative for IFN-λs in the following experiments.

In a coculture with JFH-1-infected Huh7.5.1 cells, BDCA3$^+$ DCs profoundly released IL-29, IL-28A, and IL-28B (Fig. 4D, the results of IL-29 and IL-28A, not shown), whereas BDCA3$^+$ DCs failed to respond to Huh7.5.1 cells lacking HCV/JFH-1, showing that IL-28B production from BDCA3$^+$ DCs is dependent on HCV genome (Fig. 4D). In the absence of BDCA3$^+$ DCs, IL-28B is undetectable in the supernatant from JFH-1-infected Huh7.5.1 cells, demonstrating that BDCA3$^+$ DCs, not HCV-replicating Huh7.5.1 cells, produce detectable amount of IL-28B (Fig. 4D). In the coculture, BDCA3$^+$ DCs comparably released IL-28B either in the presence or the absence of transwells, suggesting that cell-to-cell contact between DCs and Huh7.5.1 cells is dispensable for IL-28B response (Fig. 4E). In parallel with the quantity of IL-28B in the coculture, ISG15 was significantly induced only in JFH-1-infected Huh7.5.1 cells cocultured with BDCA3$^+$ DCs (Fig. 4F). A strong induction was observed with other ISGs in JFH-1-infected Huh7.5.1 in the presence of BDCA3$^+$ DCs, such as IFIT1, MxA, RSD2, IP-10, and USP18 (Fig. S7). The results clearly show that BDCA3$^+$ DCs are capable of producing large amounts of IFN-λs in response to cellular or cell-free HCV, thereby inducing various ISGs in bystander liver cells.

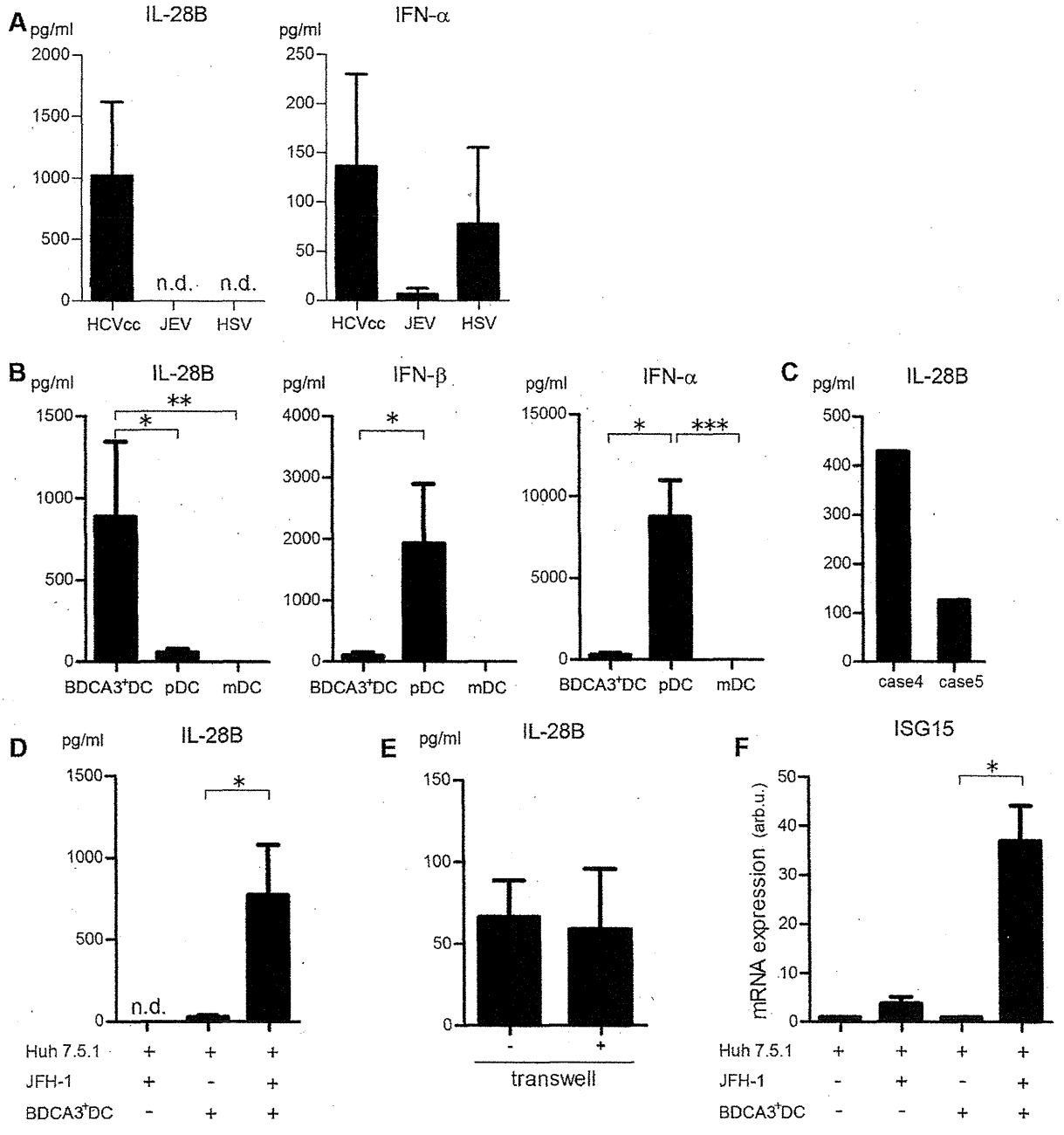

Fig. 4. BDCA3$^+$ DCs produce IL-29, IL-28A, and IL-28B upon cell-cultured HCV or HCV/JFH-1-transfected Huh7.5.1 cells, thereby inducing ISG. (A) BDCA3$^+$ DCs were cultured at 2.5 $\times$ 10^4 cells for 24 hours with HCVcc, JEV, or HSV at a multiplicity of infection (MOI) of 10. Results are shown as mean $\pm$ SEM from six experiments. n.d.; not detected. (B) BDCA3$^+$ DCs, pDCs, and mDCs were cultured at 2.5 $\times$ 10^4 cells for 24 hours with HCVcc at an MOI of 10. The results are shown as mean $\pm$ SEM from 11 experiments. *$P < 0.05$; **$P < 0.0005$; ***$P < 0.0005$ by Kruskal-Wallis test. (C) BDCA3$^+$ DCs recovered from intrahepatic lymphocytes were cultured at 2.5 $\times$ 10^4 cells for 24 hours with HCVcc at an MOI of 10. Both of the samples (cases 4 and 5) were obtained from patients with non-B, non-C liver disease. (D,E) BDCA3$^+$ DCs were cocultured at 2.5 $\times$ 10^4 cells with JFH-1-transfected (MOI = 2) or -untransfected Huh7.5.1 cells for 24 hours. The supernatants of JFH-1-transfected Huh7.5.1.cells without BDCA3$^+$ DCs were also examined. In some experiments of the coculture with JFH-1-transfected Huh7.5.1 cells and BDCA3$^+$ DCs, transwells were inserted into the wells (E). Results are shown as mean $\pm$ SEM from five experiments. *$P < 0.05$ by paired t test. (F) BDCA3$^+$ DCs were cocultured at 2.5 $\times$ 10^4 cells with JFH-1-transfected Huh7.5.1 cells (MOI = 2) or -untransfected Huh7.5.1 cells for 24 hours. The Huh7.5.1.cells were harvested and subjected to real-time RT-PCR analyses for ISG15 expression. The results are shown as mean $\pm$ SEM from five experiments. *$P < 0.05$ by paired t test. HCVcc, cell-cultured HCV; JEV, Japanese encephalitis virus; HSV, herpes simplex virus.